

Wide Field CCD photometry around nine open clusters

Saurabh Sharma¹, A. K. Pandey¹, K. Ogura², H. Mito³, K. Tarusava³ and R. Sagar¹

Received/ Accepted

ABSTRACT

In this paper we study the evolution of core and corona of nine open clusters using the projected radial density profiles derived from homogeneous CCD photometric data obtained through the 105-cm Kiso Schmidt telescope. The age and galactocentric distance of the target clusters varies from 16 Myr to 2000 Myr and 9 kpc to 10.8 kpc respectively. Barring Be 62, which is young open cluster, other clusters show a uniform reddening across the cluster region. The reddening in Be 62 varies from $E(B-V)_{min}=0.70$ mag to $E(B-V)_{max}=1.00$ mag. The corona of six of the clusters in the present sample is found to be elongated, however on the basis of the present sample it is not possible to establish any correlation between the age and shape of the core. The elongated core in the case of young cluster Be 62 may reflect the initial conditions in the parental molecular cloud. The other results of the present study are (i) Core radius ' r_c ' and corona size ' r_{cn} '/cluster radius ' r_{cl} ' are linearly correlated. (ii) The $r_c/r_{cn}/r_{cl}$ are linearly correlated with the number of stars in that region. (iii) In the age range 10-1000 Myr, the core and corona shrink with age. (iv) We find that in the galactocentric distance range 9 - 10 kpc, the core and corona/cluster extent of the clusters increase with the galactocentric distance.

Subject headings: open clusters and associations: general — techniques: photometric

1. INTRODUCTION

The study of galactic open clusters is of great interest in several astrophysical aspects. Young open clusters provide information about current star formation processes and are key

¹Aryabhatta Research Institute of Observational Sciences, Nainital, India - 263 129

²Kokugakuin University, Higashi, Shibuya-ku, Tokyo 150-8440, Japan

³Kiso Observatory, School of Science, University of Tokyo, Mitake-mura, Kiso-gun, Nagano 397-0101, Japan

objects for clarifying questions of galactic structure, while observations of old and intermediate age open cluster play an important role in studying the theories of stellar and galactic evolution.

The nucleus and the corona (extended region of the star cluster) are two main regions in open clusters (Khlopov 1969). The nucleus of a cluster contains relatively bright and massive ($\geq 3 M_{\odot}$) stars whereas corona, which contains a large number of faint and low mass ($\leq 1 M_{\odot}$) stars, has important bearing on studies related to the mass function (MF), the structure and the evolution of open clusters. A detailed analysis of the structure of corona of open clusters is needed to understand the effects of external environments like the galactic tidal field and impulsive encounters with interstellar clouds etc. on dynamical evolution of open clusters (Pandey et. al. 1990). Extensive studies of the coronal regions of clusters have not been carried out so far mainly because of non-availability of photometry in a large field around open star clusters.

The $2K \times 2K$ CCD mounted on Schmidt telescopes (Kiso, Japan), covering $\sim 50' \times 50'$ field can be used to get photometry in a large field around open star clusters. The ability to obtain improved photometry of thousands of stars means that large-scale studies of open clusters can be conducted to study the spatial structure and stability of galactic open clusters. With the addition of photometry of nearby field region, it is possible to construct luminosity function (LF)/mass function (MF), which are useful to understand the cluster-formation processes and the theory of star formation in open clusters (Miller & Scalo 1979).

Considering the importance of low mass stars in the corona of star clusters, we have generated wide field photometric database around 9 open star clusters with the aim to re-investigate the cluster's parameters e.g. reddening, distance, age, their size and LF/MF using a homogeneous data base. The basic parameters of the cluster taken from WEBDA¹ (Mermilliod 1995) are given in Table 1.

2. OBSERVATIONS AND DATA REDUCTIONS

The broad band CCD photometric observations of clusters were carried out during 2001 November 19 to 2001 November 25 using the 105 cm Schmidt telescope of the Kiso Observatory. The CCD camera used a SITe 2048×2048 pixel² TK2048E chip having a pixel size $24 \mu\text{m}$. At the Schmidt focus ($f/3.1$) each pixel of CCD corresponds to $1.^{\prime\prime}5$ and the entire chip covers a field of $\sim 50' \times 50'$ on sky. The read out noise and gain of the CCD are

¹<http://obswww.unige.ch/webda>

$23.2\text{ }e^-$ and $3.4\text{ }e^-/\text{ADU}$ respectively.

The observations of NGC 1528, NGC 2287, NGC 2301, NGC 2323, NGC 2420, NGC 2437 and NGC 2548 were standardized by observing standard stars in SA95 (Landolt 1992) having brightness $12.2 < V < 15.6$ and color $0.45 < (B - V) < 1.51$ on four nights during 2001 November 22 to 2001 November 25. To standardize the observation of Be 62 and NGC 1960 we generated secondary standard in the field of these two clusters by observing stars in SA95 on 2001 November 24 and 2001 November 22 respectively. A number of bias and dome flat frames were also taken during the observing runs. The log of observations is given in Table 2. A number of short and deep exposure frames have been obtained for all the clusters.

The CCD data frames were reduced using computing facilities available at Aryabhatta Research Institute of Observational Sciences (ARIES), Nainital. Initial processing of the data frames was done using the IRAF² and ESO-MIDAS³ data reduction packages. Photometry of cleaned frames was carried out using DAOPHOT-II software (Stetson 1987). The PSF was obtained for each frame using several uncontaminated stars. The FWHM of the star images varied between $3''$ to $4''$ from night to night. When brighter stars were saturated on deep exposure frames, their magnitude has been taken from short exposure frames. We used DAOGROW program for construction of an aperture growth curve required for determining the difference between aperture and profile fitting magnitude. Calibration of the instrumental magnitude to standard system was done using procedure outlined by Stetson (1992). The photometric calibration equations used are as follow:

$$\begin{aligned} u &= U + c_1 + m_1(U-B) + k_u X, \\ b &= B + c_2 + m_2(B-V) + k_b X, \\ v &= V + c_3 + m_3(V-I) + k_v X, \\ r &= R + c_4 + m_4(V-R) + k_r X, \\ i &= I + c_5 + m_5(V-I) + k_i X, \end{aligned}$$

where U, B, V, R and I are the standard magnitudes, u, b, v, r and i are the instrumental magnitudes normalized for 1 second of exposure time and X is the air mass; the c_1, c_2, c_3, c_4, c_5 and m_1, m_2, m_3, m_4, m_5 are zero-point constants and color-coefficients respectively; and k_u, k_b ,

²IRAF is distributed by National Optical Astronomy Observatories, USA

³ESO-MIDAS is developed and maintained by the European Southern Observatory.

k_v, k_r, k_i are extinction coefficients in U, B, V, R and I bands respectively. The values of zero-point constants, color coefficients and extinction coefficients in various bands on different nights are given in Table 3. Figure 1 shows the standardization residual, Δ , between standard and transformed V magnitude and $(U - B)$, $(B - V)$, $(V - R)$ and $(V - I)$ colors of standard stars. The standard deviations in ΔV , $\Delta(U - B)$, $\Delta(B - V)$, $\Delta(V - R)$ and $\Delta(V - I)$ are 0.017, 0.060, 0.028, 0.023, 0.020 mag respectively. The typical DAOPHOT errors in magnitude and colors along with parameter χ and sharpness as a function of V magnitude in the case of clusters Be 62 and NGC 1960 are shown in Figure 2. It can be seen that the errors become larger (≥ 0.1 mag) for stars fainter than $V = 20$ mag, therefore the measurements below this magnitude are not reliable.

3. COMPARISON WITH PREVIOUS STUDIES

We have carried out a comparison of the present data with that available in the literature. The difference Δ (literature - present data) as a function of V magnitude is shown in Figure 3 and the statistical results are given in Table 4. The comparison indicates rather a large scatter in Δ for photographic data as compared to the Δ values for CCD photometry. Comparison of the photometry in case of each cluster is discussed below.

Be 62: CCD V magnitude and $(B - V)$ colors obtained by Phelps & Janes (1994) are in good agreement with those obtained in the present work. However the photoelectric V magnitudes in the range 13-14 obtained by Forbes (1981) are brighter by ~ 0.13 mag than that obtained in the present work. The $(U - B)$ colors obtained in the present work for stars having $V \sim 13 - 16$ mag are redder than those reported by Phelps & Janes (1994). For stars having $V > 17$ mag, the $(U - B)$ colors obtained by Phelps & Janes (1994) show a strong variation with V magnitude and becomes redder by ~ 1.2 mag at $V \sim 18-19$ mag. Our $(U - B)$ colors for star $V=13-14$ mag are in agreement with the photoelectric observations by Forbes (1981).

NGC 1528: The V magnitude and $(B - V)$ colors obtained in the present work are in agreement with those reported by Hoag et al. (1961, hereafter H61).

NGC 1960: The comparison of present CCD photometry with the available photoelectric (Johnson & Morgan 1953) and photographic (Barkhatova et al. 1984) photometry indicates a fair agreement between the different measurements. The V magnitude and $(B - V)$ colors obtained by us for stars having $V \leq 15$ mag are in good agreement with those given by Sanner et al. (2000, CCD photometry), whereas V magnitude obtained by us for stars fainter than $V = 15$ mag are systematically fainter by ~ 0.06 mag and $(B - V)$ color shows

a trend with increasing V magnitude in the sense that colors obtained by us become redder.

NGC 2287: Photoelectric V magnitude by Eggen (1974) are in agreement with the present observations whereas photoelectric V magnitudes given by Harris et al. (1993), Ianna et. al. (1987) and H61 are systematically fainter by ~ 0.05 magnitude. The $(B - V)$ colors obtained in the present work are in agreement with those reported by Harris et al. (1993), Eggen et al. (1974) & Ianna et al. (1987). The $(B - V)$ colors obtained by H61 are systematically blue by ~ 0.06 mag than the $(B - V)$ colors reported in the present work.

NGC 2301: The V magnitude and $(B - V)$ colors obtained in the present work are in agreement with those reported in the literature. The $(U - B)$ colors for stars having $V \leq 16$ mag by Kim et al. (2001) are in agreement with the present results, whereas stars having $V > 16$ mag show a trend in $(U - B)$ color in the sense that present colors become bluer with increasing V magnitude. The $(U - B)$ photographic colors reported by Mohan & Sagar (1988) at $V \sim 10\text{--}13$ mag are systematically redder by ~ 0.12 mag and become further red with increasing V magnitude. Whereas, photographic $(U - B)$ colors for stars having $V = 13\text{--}15$ mag by H61 are systematically redder by ~ 0.12 mag.

NGC 2323: The comparison indicates that the V magnitude obtained by us are in general in agreement with those given in literature barring the magnitudes given by H61. The V magnitudes reported by H61 are fainter by ~ 0.06 mag. The $(B - V)$ colors also show a fair agreement with the values reported in the literature excepting $(B - V)$ colors for $V \geq 13.0$ mag given by H61 which are bluer by ~ 0.07 mag. The $(U - B)$ colors given in the literature also show a fair agreement with those obtained in the present study.

NGC 2420: The comparison of present CCD observations indicates a good agreement with those reported in the literature.

NGC 2437: The comparison of the present CCD photometry with the available photographic, photoelectric and CCD photometry indicates a good agreement between various reported observations.

NGC 2548: The photoelectric V magnitude by Pesch (1961) and Oja (1976) are systematically faint by about 0.05 magnitude.

4. ANALYSIS

4.1. Radial stellar surface density and cluster radius

As the area of present CCD observations is quite large, it can be used to study the radial extent, structure (core and corona region) and evolutionary aspects of clusters. Since, the projected distribution of stars in a cluster follows systematic distribution from the center to the outer region, the center of the cluster was estimated by convolving a Gaussian kernel with the stellar distribution and taking the point of maximum density as the center. This was performed for both the axis to get the center coordinates of the clusters. To determine the radial surface density, the cluster was divided into a number of concentric rings. Projected radial stellar density in each concentric circle was obtained by dividing the number of stars in each annulus by its area, and the same are plotted in Figure 4 for various magnitude levels. The error bars derived assuming that the number of stars in each annulus follows the Poisson statistics. The extent of the cluster ‘ r_{cl} ’ is defined as the point where the radial density becomes constant. The horizontal dashed line in the plots indicates the density of contaminating field stars, which is obtained from the region outside (about 1.5 cluster radius) the cluster area.

To check whether the density distribution shown in the left panel of Figure 4 is affected by contamination due to field stars, we selected a sample of stars near a well defined main sequence (MS) in the color-magnitude diagram (CMD) as mentioned by Pandey et al. (2001). The radial density distribution of the MS sample is also shown in the right panel of Figure 4. Both the samples in general show almost similar radial density profiles.

The observed radial density profile of the clusters was parametrized following the approach by Kaluzny & Udalski (1992) where projected radial density $\rho(r)$ is described as:

$$\rho(r) \propto \frac{f_0}{1 + \left(\frac{r}{r_c}\right)^2},$$

where the clusters core radius ‘ r_c ’ is the radial distance at which the value of $\rho(r)$ becomes half of the central density f_0 . The best fit obtained by χ^2 minimization technique is shown in Figure 4. Within uncertainties the King model (King 1962) reproduces well the radial density profiles (RDPs) of the clusters studied in the present work. Structural parameters obtained by fitting the King model surface density profile to the observed radial density profile of main sequence stars having $V < 18$ mag are given in Table 5.

Majority of the clusters indicate an increase in core radius when fainter cluster members included in the radial density profile, however two clusters namely NGC 1960 (log age \sim

7.4) and NGC 2437 (log age ~ 8.4) yield a smaller r_c toward fainter magnitude. Whereas clusters NGC 2301 (log age ~ 8.2) and NGC 2420 (log age ~ 9.3) do not show any significant change in core radius as a function of brightness of the cluster stars. The radial stellar surface density profiles displayed in Figure 4 indicate that field star contamination is not significant up to $V \sim 18$ mag, however it increases significantly at $V = 20$ mag. We expect for the sample brighter than $V \sim 18$ mag field star contamination is not strong enough to smear the cluster properties and hence will have insignificant effect in the results derived below. Poor radial surface density profile in the case of NGC 2287 is due to lack of clustering in the object.

Recently various authors have used Two Micron All Sky Survey (2MASS) data to study the radial structures of open clusters (Chen et al. 2004, hereafter C04; Bonatto & Bica 2005, hereafter BB05). We also used 2MASS data to obtain the radial density profile curve of the clusters studied in the present work and the same are shown in the lowermost panels of Figure 4. The core radius ‘ r_c ’ and extent of the cluster ‘ r_{cl} ’ of the target open clusters estimated from the projected radial density profile for main-sequence band stars are given in Table 5. Table 5 indicates that the r_c and r_{cl} obtained using the 2MASS data are larger, in some cases, than that obtained from optical data. The error in r_c obtained from 2MASS data is also relatively large in comparison to that for optical data. Various recent estimates of radii of target clusters are given in Table 6, which indicates a fare agreement between present optical estimates and those by Nilakshi et al. (2002, hereafter N02). To study various parameters, e.g. interstellar reddening, age, distances etc, in detail, we considered only those stars which are inside the cluster extent as determined from radial density profile.

4.2. Isodensity contours

It is well known that the internal interaction of two body relaxation due to encounters among member stars and external tidal forces due to the galactic disk or giant molecular clouds influence the morphology of the clusters. To study the effects of external forces on the morphology of the clusters, we obtained isodensity contours for the sample of MS stars ($V \leq 18$ mag) and the contours are shown in Figure 5. The isodensity contours are least square fitted with ellipse to obtain the elongation of the corona of the clusters. The elongation parameter ‘ e_p ’ is defined as $e_p = b/a$, where a and b are semi-major and semi-minor axis of the ellipse. The parameter e_p for each cluster is given in Figure 5. $e_p = 1$ indicates a spherical cluster. The fitting could not be done in the case of Be 62 and NGC 1960. However a visual inspection of density contours of these two clusters indicates an elongated corona of the clusters. C04 have also reported an elongated corona in the case of NGC 1960.

Figure 5 indicates that outer region (corona) of six clusters is found to be elongated. The elongated morphology in the case of NGC 2287, NGC 2548 (Bergond et al. 2001, hereafter B01) and NGC 1893, Be 17, NGC 2420 (C04) have already been reported in the literature. Present results further support the elongated morphology of the coronal region of the clusters.

4.3. Interstellar Extinction

The extinction towards the clusters Be 62, NGC 1960, NGC 2301 and NGC 2323 was estimated using the $(U - B)/(B - V)$ two color diagram shown in Figure 6. We compared observed main-sequence (MS) in the cluster region with the intrinsic MS to estimate the value of reddening $E(B - V)$. In Figure 6, we show intrinsic MS for $Z = 0.02$ by Schmidt-Kaler (1982) shifted along the reddening vector having a normal slope of $E(U - B)/E(B - V) = 0.72$. The interstellar extinction in the case of other five clusters NGC 1528, NGC 2287, NGC 2420, NGC 2437 and NGC 2548 was estimated using the $V/(B - V)$ or $V/(V - I)$ color-magnitude diagrams (CMDs, cf. § 4.4). The estimated values of $E(B - V)$ are given in Table 7 which are in good agreement with those given in the literature. Barring the cluster Be 62, all other clusters show a uniform reddening across the cluster region. The reddening in Be 62 varies from $E(B - V)_{min} = 0.70$ mag to $E(B - V)_{max} = 1.00$ mag. The reddening for individual stars ($V_{error} \leq 0.1$ mag) having spectral type earlier than A0 has also been derived using the Q-method (Johnson & Morgan 1953).

To study the nature of the extinction law in the cluster region, we used two-color diagrams (TCDs) as described by Pandey et al. (2001, 2003). The TCDs of the form of $(\lambda - V)$ vs. $(B - V)$, where $(\lambda - V)$ is one of the wavelength of the broadband filters (R, I, J, H, K, L) provide an effective method for separating the influence of the normal extinction produced by the diffuse interstellar medium from that of the abnormal extinction arising within regions having a peculiar distribution of dust sizes (cf. Chini & Wargan 1990, Pandey et al. 2000). The near infrared (NIR) data have been taken from the 2MASS. For illustration, the TCDs for the clusters Be 62, NGC 2420 and NGC 1960 are shown in Figure 7 and slopes of the distribution, $m_{cluster}$, in the case of these three clusters are given in Table 8.

The $\frac{E(\lambda - V)}{E(B - V)}$ values in the cluster region are estimated using the following approximate relation:

$$\frac{E(\lambda - V)}{E(B - V)} = \frac{m_{cluster}}{m_{normal}} \times \left[\frac{E(\lambda - V)}{E(B - V)} \right]_{normal}$$

as described by Pandey et al. (2003), where $m_{cluster}$ and m_{normal} are the slope of the distribution in the cluster region and slope of the theoretical MS. The slopes of the theoretical MS, m_{normal} , obtained from the stellar models by Bertelli et al. (1994) are also given in Table 8. The obtained slope $m_{cluster}$ indicates that barring Be 62 and NGC 2420 all other clusters show a normal reddening law towards the cluster region. The color excess ratio $\frac{E(\lambda-V)}{E(B-V)}$ for Be 62 and NGC 2420 are smaller than the normal ones, which indicates that there may be anomalous reddening law towards these cluster regions. Since Be 62 shows a differential extinction indicating that the stars are still embedded in the parent molecular gas and dust, an anomalous reddening law is expected in the cluster region. The value of R towards the cluster Be 62 region estimated to be 2.95 ± 0.12 . However it is quite surprising in the case of NGC 2420 which is an old cluster having a uniform reddening across the cluster. Keeping the large error in mind we used a normal value of R for all the cluster regions in the ensuing discussions.

4.4. Color magnitude diagrams, distance and age of the clusters

Color magnitude diagrams (CMDs) for stars lying within cluster region as mentioned in Table 5 are shown in Figure 8. The CMDs show a well defined MS. Barring Be 62, other clusters manifest a uniform reddening in the cluster region and the error in magnitude estimation is ~ 0.05 mag for stars having $V \leq 18.0$ mag. Therefore we can conclude that the presence of probable binaries and field stars should be the main cause for broadening of the MS in these clusters. In the case of Be 62 variable reddening in the cluster region along with presence of probable binaries and field stars should be the cause of broad MS. It is difficult to separate field stars from the cluster stars, however we can reduce the contamination due to field stars if we restrict the sample to the central portion of the cluster only.

We supplemented present CCD data for some cluster with the photoelectric photometry for bright stars available in the literature as these bright stars were saturated even on present short exposure frames. The distance and age of the cluster were obtained by visual fitting of isochrones by Bertelli et al. (1994) for $Z = 0.02$ to the blue envelope of the observed MS except in the case of NGC 2420 where we used isochrones for $Z = 0.008$ as Lee et al. (2002) have reported $Z = 0.009$ for the cluster NGC 2420. The fitted isochrones are shown in Figure 8. Since extinction is uniform in clusters under study except Be 62, we used mean value of $E(B-V)$ and following relations, $E(U-B)/E(B-V)=0.72$, $A_V = 3.1 \times E(B-V)$, $E(V-R) = 0.60 \times E(B-V)$, $E(V-I) = 1.25 \times E(B-V)$ to fit the theoretical isochrones to the observations. In the case of Be 62 individual reddening for stars earlier than $A0$ was obtained using the Q method and the same was applied to get intrinsic magnitude and

colors, whereas for other stars mean reddening of the nearby stars was applied to get the intrinsic magnitude and colors. The unreddened CMDs along with the fitted isochrones in the case of Be 62 are shown in Figure 9. The age and distance obtained for the target clusters are given in Table 8. The $K/(J - K)$ CMDs for the clusters obtained from 2MASS data are shown in Figure 10. The theoretical isochrones by Bertelli et al. (1994) using the parameters obtained from the optical data (cf. Table 7) are also plotted in Figure 10 which nicely follow the observations. Comparison of previous estimates available in the literature with the present estimates is given in Table 9.

5. RESULTS

We have determined basic parameters of 9 open clusters by analyzing the color-color diagrams and CMDs of the clusters. We assumed solar abundance for all the clusters except NGC 2420 where metallicity is reported to be $Z = 0.009$ by Lee et al. (2002). The discussion on individual cluster follows, where we have compared the radii of the cluster obtained in the present study with those reported by N02, BB05, C04 and Kharchenko et al. (2005, hereafter K05). The morphological parameters of open clusters derived by N02 and K05 are based on optical observations whereas C04 and BB05 have used 2MASS data. In the subsequent sections we use the core radius ' r_c ' and cluster extent ' r_{cl} ' obtained from the present optical photometric and 2MASS data.

5.1. Be 62

The reddening $E(B - V)$, distance and age for the cluster has been estimated as 0.86 mag, 2.05 ± 0.24 kpc and 10 Myr by Forbes (1981) using the photoelectric photometry, whereas Phelps & Janes (1994) using the CCD observations reported $E(B - V) = 0.82$ mag, distance = 2.7 kpc and an age of ~ 10 Myr for this cluster.

In Figure 8, $V/(B - V)$, $V/(V - R)$, $V/(V - I)$ CMDs for stars within the cluster region i.e. $r_{cl} = 10.0'$ (6.8 pc) are presented. The CMDs of the Be 62 shows a broad MS which should be due to variable reddening in the cluster region. To get unreddened CMDs, the reddening $E(B - V)$ for stars having spectral type A0 or earlier has been calculated using the Q method and these stars were unreddened individually. For remaining stars the average reddening of the nearby stars was applied. The unreddened CMDs shown in Figure 9. To calculate V_O , the value of $R = 3.1$ is assumed. The distance and age of the cluster comes out to be 2.32 kpc and 16 Myr ($\log \text{age} = 7.2$). The distance obtained in the present work is

in between the values 2.05 kpc and 2.70 kpc reported by Forbes (1981) and Phelps & Janes (1994) respectively.

The core of the cluster using the optical MS data is estimated to be $\sim 2.^{\circ}2 \pm 0.^{\circ}3$ (1.5 ± 0.2 pc). The 2MASS data gives the value for core as $\sim 2.^{\circ}5 \pm 1.^{\circ}0$ (1.7 ± 0.7 pc). The optical and 2MASS data yields the extents of cluster as $\sim 10'$ (6.8 pc) and $\sim 12'$ (8.1 pc) respectively. The core and the coronal region of the cluster are found to be elongated.

5.2. NGC 1528

The radial density profile of the cluster yields its extent $r_{cl} \sim 15'$ (4.8 pc) with a core radius $r_c \sim 8.^{\circ}3 \pm 1.^{\circ}5$ (2.6 ± 0.5 pc) which is in agreement with the value ($8.^{\circ}4$) by K05, however the r_{cl} obtained in the present work ($\sim 15'$) is significantly smaller than the value ($26.^{\circ}4$) by K05. The RDP obtained using the 2MASS data is quite noisy and it yields significantly different value of r_c ($\sim 18.^{\circ}5 \pm 7.^{\circ}4$; 5.9 ± 2.4 pc).

The CMDs of the cluster within $r_{cl} \sim 15'$ show a well defined but broad MS. Since the cluster has uniform reddening, the presence of binary stars should be a probable reason for the broadening of the MS. The CMDs show the turn-off of the MS which can be fitted nicely with a isochrones of $\log \text{age} = 8.6$ (400 Myr) and $Z = 0.02$. The distance to the cluster comes out to be 1.09 kpc which is in agreement with those reported in the literature. Isodensity curves shown in Figure 5 indicate that both the core and the corona have elongated morphology.

5.3. NGC 1960 (M36)

This cluster situated in Auriga constellation is reported to have diameter of $10'$ (Lynga & Palous 1987). Sanner et al. (2000) reported a distance modulus $(m - M)_o = 10.6 \pm 0.2$ mag (1318 ± 120 pc), reddening $E(B - V) = 0.25 \pm 0.02$ mag, age = 16^{+10}_{-5} Myr and metallicity $Z = 0.02$ for the cluster.

The CMDs of the NGC 1960 show a well defined narrow MS. By fitting the isochrones for $\log \text{age} = 7.4$ (25 Myr) to the stellar distribution in the CMDs using $E(B - V) = 0.22$ mag, we obtained a distance modulus $(m - M)_V = 11.3$ mag corresponding to a true distance modulus $(m - M)_o = 10.62$ mag, or a distance of 1.33 kpc. The estimated age, distance and reddening in the cluster region are in good agreement with the values obtained in earlier studies (e.g. Sanner et al. 2000).

The core radius ($r_c \sim 3.^{\circ}2 \pm 0.^{\circ}5$; 1.2 ± 0.1 pc) and cluster extent ($r_{cl} \sim 14'$; 5.4 pc) obtained in the present study are in good agreement with the values obtained by N02 ($r_c \sim 3.^{\circ}2$, $r_{cl} \sim 15.^{\circ}4$). The core radius ($r_c \sim 5.^{\circ}4$) obtained by K05 is larger than the present value. The cluster extent ($r_{cl} \sim 14'$) obtained in the present work is in agreement with the value ($\sim 16.^{\circ}2$) by K05 whereas it is larger than that ($\sim 7.^{\circ}6$) reported by C04. From 2MASS data, we obtained $r_c \sim 3.^{\circ}8 \pm 0.^{\circ}6$ (1.5 ± 0.2 pc) and $r_{cl} \sim 21'$ (8.1 pc). The core of the cluster is rather spherical symmetric whereas the outer region of the cluster clearly shows the effect of external forces.

5.4. NGC 2287 (M41)

Despite being a bright cluster, no CCD photometry is available for this cluster. This cluster has been studied for proper motion (Ianna et al. 1987), radial velocities (Amieux 1988) and spectroscopic properties (Harris et al. 1993). Battinelli et al. (1994) and B01 have reported $R_{lim} = 4.0$ pc ($19'$) and $R_{tidal} = 4.1$ pc ($20.^{\circ}3$) respectively for the cluster. K05 have reported $r_c \sim 9.^{\circ}6$ and $r_{cl} \sim 30'$. BB05 have estimated $R_{core} = 1.1$ pc ($4.^{\circ}7$) and $R_{lim} = 7.0$ pc ($30.^{\circ}1$). In present study we found that optical data for brighter limiting visual magnitude ($V \sim 14$ mag) and fainter limiting magnitude ($V \leq 18$ mag) were yielding quite different values for the morphology of the cluster. For brighter sample we obtained $r_c \sim 5.^{\circ}5 \pm 0.^{\circ}9$ (1.1 ± 0.2 pc), $r_{cl} \sim 17'$ (3.5 pc) whereas for sample having $V \leq 18$ mag these values are estimated as $\sim 1.^{\circ}4 \pm 0.^{\circ}3$ (0.3 ± 0.2 pc) and $\sim 12'$ (2.5 pc) respectively. The radial density profile for 2MASS data is quite noisy with $r_c \sim 12.^{\circ}7 \pm 3.^{\circ}8$ (2.6 ± 0.8 pc) and $r_{cl} \sim 16'$ (3.3 pc). For further study of the cluster, we assumed $r_{cl} \sim 12'$ (2.5 pc). The morphology of the cluster indicates that both the central region and outer region are elongated. The center coordinate for the cluster reported by B01 are shifted towards $15'$ SW of “classical” coordinates given in WEBDA. However, BB05 find the same coordinates for the center as given in WEBDA, whereas in the present work we find a shifted center for the cluster towards north of the center as given in WEBDA.

The CMDs of the clusters show a very well defined MS along with red giant clump. The distance and age for the cluster estimated to be 0.71 kpc and 250 Myr ($\log \text{age} = 8.4$) which are in agreement with recent findings.

5.5. NGC 2301

A comparison of the theoretical isochrones with the observations yields a distance modulus $(m - M)_V = 9.8$ mag, which corresponds to a true distance modulus $(m - M)_0 = 9.71$ mag or a distance of 0.87 kpc and an age of 160 Myr (\log age = 8.2) for the cluster. The age, distance and reddening towards the cluster region obtained in the present work are in good agreement with those reported in the literature.

The estimated core radius ($r_c \sim 1.^{\circ}9 \pm 0.^{\circ}3$; 0.5 ± 0.1 pc) is in good agreement with the value ($r_c \sim 1.^{\circ}9$; 0.5 pc) by N02 whereas it is significantly smaller than $r_c \sim 4.^{\circ}8$ by K05. The extent of cluster ($\sim 9'$; 2.3 pc) obtained in the present work is smaller than that reported by N02 ($12'$; 3.0 pc) and K05 ($\sim 15'$). Here it is worthwhile to mention that the core radius ($r_c \sim 4.^{\circ}5 \pm 1.^{\circ}0$; 1.1 ± 0.2 pc) and cluster extent ($r_{cl} \sim 20'$; 5.1 pc) obtained from the 2MASS data are almost double to that values obtained from the optical observations. The core and coronal region of the cluster NGC 2301 are found to be highly elongated indicating a strong effect of external forces on the cluster.

5.6. NGC 2323 (M50)

The distribution of MS stars having $V \leq 18$ mag yields $r_c \sim 6.^{\circ}5 \pm 1.^{\circ}5$ (1.8 ± 0.4 pc) and $r_{cl} \sim 17'$ (4.7 pc). The core radius obtained in the present study is larger than that obtained by N02 ($2.^{\circ}6$) but in agreement with that obtained by K05 ($6'$). The extent of the cluster is in agreement with that reported by N02 ($16.^{\circ}7$), however it is smaller than that reported by K05 ($\sim 22.^{\circ}2$). The 2MASS data yield $r_c \sim 6.^{\circ}7 \pm 1.^{\circ}3$ (1.9 ± 0.4 pc) and $r_{cl} \sim 22'$ (6.1 pc). The radial density profile derived from optical and 2MASS data thus gives comparable core radius. The core and the coronal region of the cluster are found to be spherical.

The cluster NGC 2323 shows a well defined MS towards the brighter end ($V \leq 15$ mag). The effect of photometric error becomes significant towards the fainter end. A comparison of the observations with the theoretical isochrones yields a distance of 0.95 kpc and age of ~ 100 Myr (\log age = 8.0) to the cluster.

5.7. NGC 2420

The BV and VI CCD photometry for the cluster NGC 2420 has been carried out by Anthony-Twarog et al. (1990) and Lee et al. (2002) respectively. Leonard (1988), using the star counts on Palomar Sky Survey, reported a quite large extent of $\sim 20'$ for the cluster.

In the present work we find that optical data and 2MASS data indicate a radial extent of the cluster is $\sim 10'$ (7.2 pc) and $\sim 9'$ (6.5 pc) respectively which is in fair agreement with that reported by C04 ($\sim 11.'$ 6) but smaller than that reported by N02 ($\sim 13.'$ 2). The core radius is estimated to be $1.'4 \pm 0.'1$ (1.0 ± 0.1 pc) which is in agreement with that obtained by N02 ($1.'5$). 2MASS data also yield nearly same core radius $\sim 1.'3 \pm 0.'2$ (0.9 ± 0.1 pc). The isodensity curves indicate a rather spherical core and coronal regions of the cluster. C04 have obtained a spherical core with an elongated coronal region of the cluster.

The CMDs within the cluster region displayed in Figure 8 show a well defined MS. As can be seen in the CMDs, the contamination due to field stars is almost negligible. The CMDs manifest a sequence of evolved stars which is nicely reproduced by the theoretical isochrones for $Z = 0.008$ and $\log \text{age} = 9.3$ (2 Gyr).

The distance to the cluster is estimated to be 2.48 kpc, which is in good agreement with the values reported by Anthony-Twarog et al. (1990), Lee et al. (2002) and West (1967) whereas distance reported by McClure et al. (1974) is 1.9 kpc. Because of its age and metallicity, NGC 2420 is an important object to test theoretical stellar evolutionary models.

5.8. NGC 2437 (M46)

The star count peak obtained in the present work is shifted by $\sim 3'$ East and $\sim 1'$ south to the center coordinates given in WEBDA. The radial density profile obtained for optical as well as 2MASS data shows a well defined distribution of stellar density around center of the cluster. However the extent of the cluster obtained for two distributions differs. The r_{cl} estimated to be $\sim 20'$ (8.8 pc) and $25'$ (11.0 pc) for the optical and 2MASS data while the corresponding values of r_c are $6.'8 \pm 1.'0$ (3.0 ± 0.4 pc) and $9.'6 \pm 0.'6$ (4.2 ± 0.3 pc) respectively. The values of r_c reported by K05 and N02 are $7.'2$ and $5.'2$ respectively. The corresponding r_{cl} values are $22.'8$ and $26.'6$ respectively. The core of the cluster is elongated whereas the corona of the cluster is found to have spherical symmetry.

The $V/(B - V)$ and $V/(V - I)$ CMDs for the cluster indicate a broad and well defined MS. The effect of field star contamination and errors is clearly visible towards fainter end ($V > 15$ mag). A few stars on the red giant clump region can also be noticed. Using $E(B - V) = 0.10$ mag we obtained a distance of ~ 1.51 kpc and an age ~ 250 Myr ($\log \text{age} = 8.4$) for the cluster. Since the cluster is of intermediate age and no indication of presence of parental molecular gas and dust, the broad MS may be probably due to presence of binary stars.

5.9. NGC 2548 (M48)

The point of maximum stellar density i.e. adopted center of the cluster is found towards south ($\sim 1.^{\circ}6$) of the center given in WEBDA. The center reported by BB05 is in excellent agreement with that obtained in the present work. However, B01 obtained the center of this cluster further south of ($\sim 1.^{\circ}4$) of the coordinate obtained in the present work. The extent of the cluster is reported to be 4.8 pc (21.5), 8.8 pc (37.8) by B01 and BB05 respectively. K05 have reported a significantly larger value (43.8) for the cluster extent. The core radius r_c is reported as $3.^{\circ}9 \pm 0.^{\circ}9$ (0.9 ± 0.2 pc) by BB05 whereas K05 reported a significantly larger value for the core as $r_c \sim 15'$. In the present work we found $r_c \sim 1.^{\circ}5 \pm 0.^{\circ}2$ (0.3 ± 0.1 pc) and $\sim 2.^{\circ}4 \pm 1.^{\circ}5$ (0.5 ± 0.3 pc) for optical and 2MASS data respectively, whereas the extent of the cluster for both of the samples is found to be $\sim 8'$ (1.8 pc). The elongated morphology of the coronal region of the cluster manifests that cluster structure has been affected by a significant amount of external forces.

The cluster shows a well defined narrow MS in the $V/(V - I)$ CMD with a few evolved stars on the giant branch. The shape of the turn-off point is that of typical intermediate-age open cluster and can be nicely explained by an isochrones having $Z = 0.02$ and age ~ 400 Myr ($\log \text{age} = 8.6$). The distance to the cluster is estimated to be 0.77 kpc.

6. DISCUSSION AND SUMMARY

6.1. The evolution of core and corona of clusters

The isodensity curves shown in Figure 5 indicate that the coronal regions of the six clusters show an elongated morphology. The youngest cluster of the present sample, Be 62 ($\log \text{age} = 7.2$) has an elongated core, whereas NGC 1960 ($\log \text{age} = 7.4$) has somewhat spherical core. On the other hand, the core of the cluster NGC 2548 ($\log \text{age} = 8.6$) shows an elongated morphology whereas the core of the NGC 2420, oldest cluster in the present sample ($\log \text{age} = 9.3$) shows rather a spherical symmetry. C04 have also reported a spherical core in the case of NGC 2420. On the basis of present small homogeneous data sample it is not possible to establish any correlation between age and shape of the core. However C04 found that the core tends to circularize as a star cluster ages. It seems that initial morphology of the open cluster at the time of formation of the cluster is governed by the initial conditions in the parent molecular clouds (cf. C04), because observed shapes of molecular cloud cores also show highly elongated morphology (Curry 2002; Gutermuth et al. 2005). C04 suggested that the later evolution of the cluster may be governed by both the internal gravitational interaction and external tidal forces.

Danilov & Seleznev (1994) showed that the parameter ζ ($=\frac{R_1}{R_2}$) and μ ($=\frac{N_1}{N_2}$) follow the relationship $\zeta \propto \mu^{0.35}$, where R_1 and R_2 are the radii of the cluster core and halo, and N_1 and N_2 are numbers of star in the core and halo. This relationship may be caused by an approximate equality between the rates of transfer of star from the core to corona and vice-versa, as a result of stellar encounters (Danilov 1997). In order to study the core-corona structure, we selected a mass limited sample, since evolution of clusters, their stability and their parameters depend on the mass of the cluster (cf. Pandey et al. 1991; BB05). We estimated various parameters for the target clusters for mass limited sample having $M_V \leq 7$ mag and these are given in Table 10. In the case of Be 62, it is not possible to estimate the parameters for $M_V \leq 7$ mag ($V \leq 21$ mag), we used parameters obtained for $V \leq 20$ mag ($M_V \leq 6$ mag) for further analysis. Data for a few cluster studied earlier by us have been taken from literature and relevant parameters for the clusters are given in Table 11. In Figure 11 we plot $(\frac{r_c}{r_{cn}})$ vs. $(\frac{n_c}{n_{cn}})$ and $(\frac{r_c}{r_{cl}})$ vs. $(\frac{n_c}{n_{cl}})$ diagrams for the target clusters where r_c , r_{cn} ($= r_{cl} - r_c$) and r_{cl} represents core radius, size of corona and cluster extent respectively and n_c , n_{cn} and n_{cl} represents number of stars in the core, corona and cluster respectively. Figure 11a indicates that clusters under study except NGC 1528 follow the relation $(\frac{r_c}{r_{cn}}) \propto (\frac{n_c}{n_{cn}})^{0.35}$ as suggested by Danilov & Seleznev (1994). The anomalous location of NGC 1528 in Figure 11 is probably due to large error in estimating the core radius because of noisy radial density profile. If we take the core radius obtained from all star radial density profile as shown in Figure 4, the cluster follows the expected relation as shown in Figure 11. Danilov & Seleznev (1994) have carried out simulation of isolated cluster dynamics and found that the parameters ζ & μ obtained from simulations also follow the relation $\zeta \propto \mu^{0.35}$. They concluded that the evolution of the core and corona of the clusters are mainly controlled by internal relaxation processes.

In Figure 12 we plot various structural parameters of the clusters, given in Tables 10 and 11, which indicates that r_c has a good correlation with r_{cn} and r_{cl} . Similarly r_c , r_{cn} and r_{cl} indicate a linear correlation with the number of stars in the core, corona and the entire cluster in the sense larger core, corona can accommodate larger number of stars. The central density f_0 decreases exponentially with increase in core radius. In Figure 13, various structural parameters from Tables 10 and 11 are plotted as a function of age which indicate that in the age range 10-1000 Myr, the core and extent of the cluster seems to shrink with age. In the case of less massive clusters, the work of BB05 (their Figure 7g) also indicates a similar correlation between age and core radius for the cluster having age ≤ 1000 Myr. Because of the above correlation between age and core/corona radius, the projected surface density in core (ρ_c) and corona (ρ_{cn}) is higher for intermediate/old age (100-1000 Myr) clusters as compared to younger clusters. The same trend can be noticed in Figure 7i and Figure 7l of BB05 for less massive clusters. The concentration parameter r_{cl}/r_c is plotted as

a function of age in Figure 13 which indicates no trend with age. N02 have also concluded the same.

Figure 13 also indicates that the core and corona of two oldest open clusters in the present sample (age $> 10^9$ yr), namely NGC 2420 ($r_c = 1.0$ pc, $r_{cl} = 10$ pc) and Be 20 ($r_c = 1.6$ pc, $r_{cl} = 6.6$ pc), are found to be relatively larger than the expected value of r_c (~ 0.5 pc) and r_{cl} (~ 2 pc) at age $\sim 10^9$ yr. These clusters are located at large distances (NGC 2420; $z = 844$ pc & Be 20; $z = -2700$ pc) from the galactic plane. The large corona of NGC 2420 and Be 20 probably indicates that these clusters may be in process of disintegration as suggested by C04.

Dependence of cluster sizes on the galactocentric distances R_G is displayed in Figure 14. A vertical dashed line is drawn to delineate the sample of clusters having $R_G < 10$ kpc and $R_G > 10$ kpc. The figure indicates that in the range $9 < R_G < 10$ kpc, the core, corona and total cluster size increase with the galactocentric distance. The study of N02 also indicates a similar correlation between cluster size and R_G in the range $R_G > 9$ kpc.

6.2. Summary

This paper analyzes homogeneous wide field CCD data of nine open cluster (ages in the range 16 Myr to 2 Gyr) taken from Kiso Schmidt telescope. Based on the well defined $(U - B)/(B - V)$ two color diagram and CMDs, we estimated the reddening towards the cluster region, the distance and age of the target clusters. The structural parameter for target clusters were obtained using the projected radial density profile. Most of the clusters show an increase in core radius when faint cluster members included in the sample. The radial structure of all clusters can be well explained by King's empirical model (1962). The target clusters sample indicate an elongated core for young (Be 62, log age = 7.2) as well as for intermediate age open clusters (NGC 2548, log age = 8.6). C04 mentioned that the clusters have tendency towards spherical shaping away from the disk, in particular in the case of old systems due to internal dynamical relaxation. However we find that relatively young cluster NGC 1960 (log age = 7.4, $z = 24$ pc) has a rather spherical core.

Present sample of the clusters follows the relation $\frac{r_c}{r_{cn}} \propto \left(\frac{n_c}{n_{cn}}\right)^{0.35}$ as suggested by Danilov & Seleznev (1994). It is found that the core radius and corona size/cluster radius are linearly correlated. It is also found that in the age range 10-1000 Myr, the core and corona of the cluster shrink with age. In the galactocentric distance range 9-10 kpc, the core and corona/cluster extent of the clusters increase with galactocentric distance.

We would like to thank the anonymous referee for his constructive comments. This work is partly supported by the Department of Science and Technology (DST) India and Japan Society for the Promotion of Science (JSPS) Japan. AKP is thankful to the staff of KISO observatory for their help during his stay there.

REFERENCES

Amieux, G. 1988, *A&AS*, 76, 305

Anthony-Twarog, B. J., Kaluzny, J., Shara, M. M., & Twarog, B. A. 1990, *AJ*, 99, 1504

Barbaro, G., Dallaporta, N., & Fabris, G. 1969, *Ap&SS*, 3, 123

Barbaro, G., Dallaporta, N., & Nobili, L. 1967, *POPAd*, 138, 1

Barkhatova, K. A., Zakharova, P. E., Malisheva, L. K., & Shashkina, L. P. 1984, *Methods of invest. Astr. Geod. Urals Univ.*, 118

Battinelli, P., Brandimarti, A., & Capuzzo-Dolcetta, R. 1994, *A&AS*, 104, 379

Bergond, G., Leon, S., Guibert, J. 2001, *A&A*, 377, 462

Bertelli, G., Bressan, A., Chiosi, C., Fagotto, F., & Nasi, E. 1994, *A&AS*, 106, 275

Bonatto, C., & Bica, E. 2005, *A&A*, 437, 483

Cannon, R. D., & Lloyd, C. 1970, *MNRAS*, 150, 279

Chen, W. P., Chen, C. W., & Shu, C. G. 2004, *AJ*, 128, 2306

Chini, R., & Wargau, W. F. 1990, *A&A*, 227, 213

Claria, J. J., Piatti, A.E., & Lapasset, E. 1998, *A&AS*, 128, 131

Collinder, P. 1931, *AnLun*, 2, 1

Cox, A. N. 1954, *ApJ*, 119, 188

Curry, C. C. 2002, *ApJ*, 526, 849.

Cuffey, J. 1941, *ApJ*, 94, 55

Danilov, V. M., & Seleznev, A.F., 1994, *Astron. Astrophys. Trans*, 6, 85

Danilov, V. M. 1997, *ARep*, 41, 163

Durgapal, A. K., & Pandey, A. K., 2001, *A&A*, 375, 840

Eggen, O. J. 1974, *ApJ*, 188, 59

Eggen, O. J. 1975, *PASP*, 87, 37

Eggen, O. J. 1981, *ApJ*, 247, 507

Feinstein A., Claria, J. J., & Cabrera, A. L. 1978, *A&AS*, 34, 241

Francic, S. P. 1989, *AJ*, 98, 3, 888

Forbes, D. 1981, *PASP*, 93, 441

Gutermuth, R A., Megeath, S. T., Pipher, J. L., Williams, J. P., Allen, L. E., Myers, P. C., & Raines, S. N. 2005, *ApJ*, 632, 397

Harris, G. L. H., FitzGerald, M. P. V., Mehta, S., & Reed, B. C. 1993, *AJ*, 106, 1533

Henden, A. 2003, Henden field photometry, <ftp://ftp.nofs.navy.mil/pub/outgoing/aah/sequence/>

Hoag, A. A., Johnson, H. L., Iriarte, B., Mitchell, R. I., Hallam, K. L., & Sharpless, S. 1961, *PUSNO*, 17, 343

Ianna, P. A., Adler, D. S., & Faudree, E. F. 1987, *AJ*, 92, 347

Johnson, H. L., & Morgan, W. W. 1953, *ApJ*, 117, 313

Kalirai, J. S., Fahlman, G. G., Richer, H. B., & Ventura, P. 2003, *AJ*, 126, 1402

Kaluzny, J., & Udalski, A. 1992, *AcA*, 42, 29

Kholopov, P.N. 1969, *SvA-AJ* 12, 625

Kharchenko, N. V., Piskunov, A. E., Rser, S., Schilbach, E., & Scholz, R.-D. 2005, *A&A*, 438, 1163

Kim, S. L., et al. 2001, *A&A*, 371, 571

King, I. 1962, *AJ*, 67, 471

Landolt, A. 1992, *AJ*, 104, 340

Lee, S. H., Ann, H. B., & Kang, Y. W. 2002, in IAU 8th Asian-Pacific Regional Meeting, Volume II, ed. S. Ikeuchi, J. Hearnshaw, and T. Hanawa (Astronomical Society of Japan), 273

Leonard, P. J. T. 1988, *AJ*, 95, 108

Lynga, G., Palous, J. 1987, *A&A*, 188, 35

Lynga, G. 1984, Catalogue of open cluster, Centre de Donnees stellaires, Strasbourg

Mermilliod, J. C. 1995, in "Information and On-Line Data in Astronomy", ed. D. Egret & M.A. Albrecht (Kluwer Academic Press, Dordrecht), 127

Miriani, G. P., & Ursula O. R. 1983, AJ, 88, 12

McClure, R. D., Forrester, W. T., & Gibson, J. 1974, ApJ, 189, 409

McClure, R. D., Newell B., & Barnes J. V. 1978, PASP, 90, 170

Miller, G. E., & Scalo, J. M. 1979, ApJS, 41, 513

Mohan, V., & Sagar, R. 1988, BASI, 16, 159

Mostafa, A. A., Hassan, S. M., Aiad A., & Ahmed, I. 1983, J. Astron. Soc. Egypt 5, 23

Napiwotzki, R., Schönberner, D., & Weidemann, V. 1991, A&A, 243, 5

Nissen, P. E., 1988, A&A, 199, 146

Nilakshi, Sagar, R., Pandey, A. K., & Mohan, V. 2002, A&A, 383, 153

Oja, T. 1976, http://www.univie.ac.at/webda/cgi-bin/frame_detail.cgi?ngc2548

Pandey, A. K., Mahra, H. S., & Sagar, R. 1990, AJ, 99, 617

Pandey, A. K., Bhatt, B. C., & Mahra, H. S. 1991, MmSAI, 62, 927

Pandey, A. K., Ogura, K., & Sekiguchi, K. 2000, PASJ, 52, 847

Pandey, A. K., Nilakshi, Ogura, K., Sagar, R., & Tarusawa, K. 2001, A&A, 374, 504

Pandey, A. K., Upadhyay, K., Nakada, Y., & Ogura, K., 2003, A&A, 397, 191

Pandey, A. K., Upadhyay, K., Ogura, K., Sagar, R., Mohan, V., Mito, H., Bhatt, H. C., & Bhatt, B. C. 2005, MNRAS, 358, 1290

Pesch, P. 1961, ApJ, 134, 602

Phelps, R. L., & Janes, K. A. 1994, ApJS, 90, 31

Rieke, C. A. 1935, HarCi, 397, 1

Sanner, J., Altmann, M., Brunzendorf, J., & Geffert, M. 2000, A&A, 357, 471

Sarma, M. B. K., & Walker, M. F. 1962, ApJ, 135, 11

Schmidt-Kaler, Th. 1982, Landolt-Bornstein, Vol. 2b, ed. K. Schaifers, H. H. Voigt & H. Landolt (Berlin: Springer), 19

Shapley, H. 1930, Star Clusters, Appen. B.

Smyth, M.J., & Nandy, K. 1962, PROE, 3, 24

Stetson, P. B. 2000, PASP, 112, 925

Stetson, P. B. 1987, PASP, 99, 191

Stetson, P. B., 1992, in ASP Conf. Ser. Vol. 25, Astronomical Data Analysis Software and System I. Astron. Soc. Pac., ed. Warrall D.M., & Biemesderfer C., Barnes J., San Francisco, 297

Trumpler, R. 1930, LicOB, 14, 154

Twarog, B. A., Ashman, K. M., & Anthony-Twarog, B. J. 1997, AJ, 114, 2556

West, F. R. 1967, ApJS, 14, 384

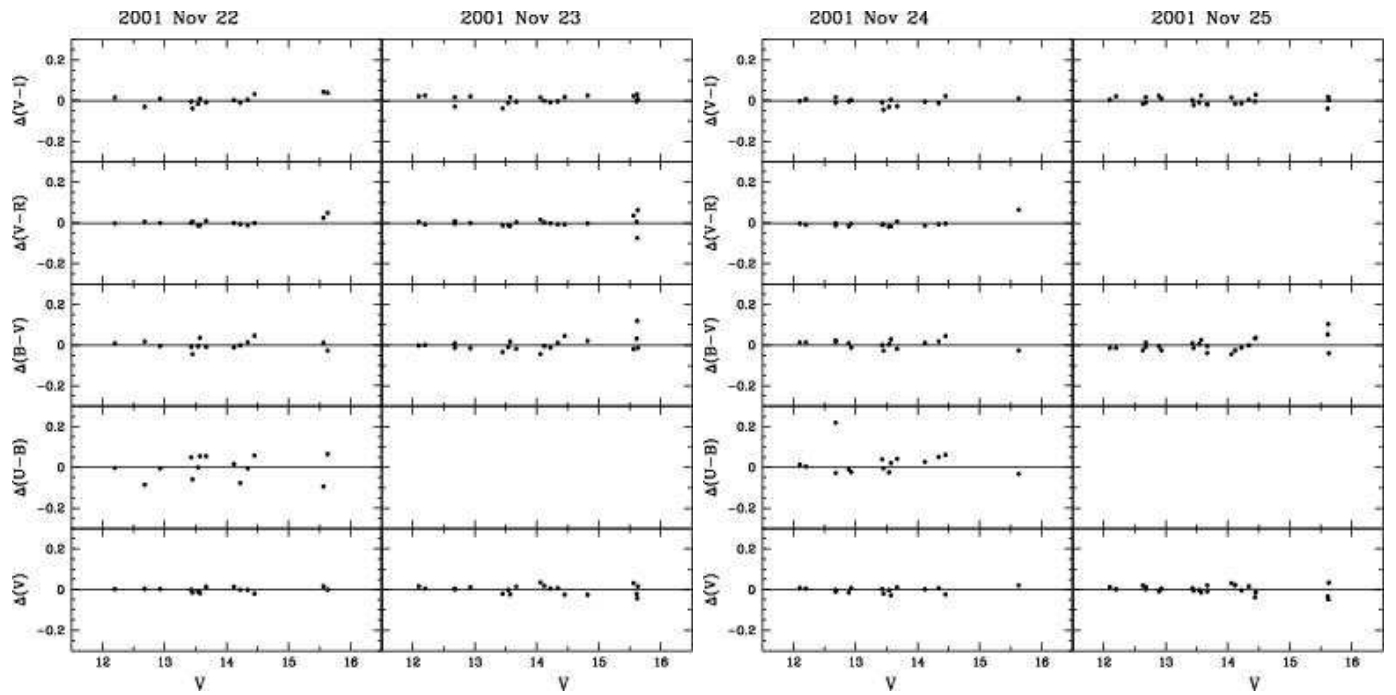


Fig. 1.— Residuals between standard and transformed magnitude and colors of standard stars plotted against standard magnitude.

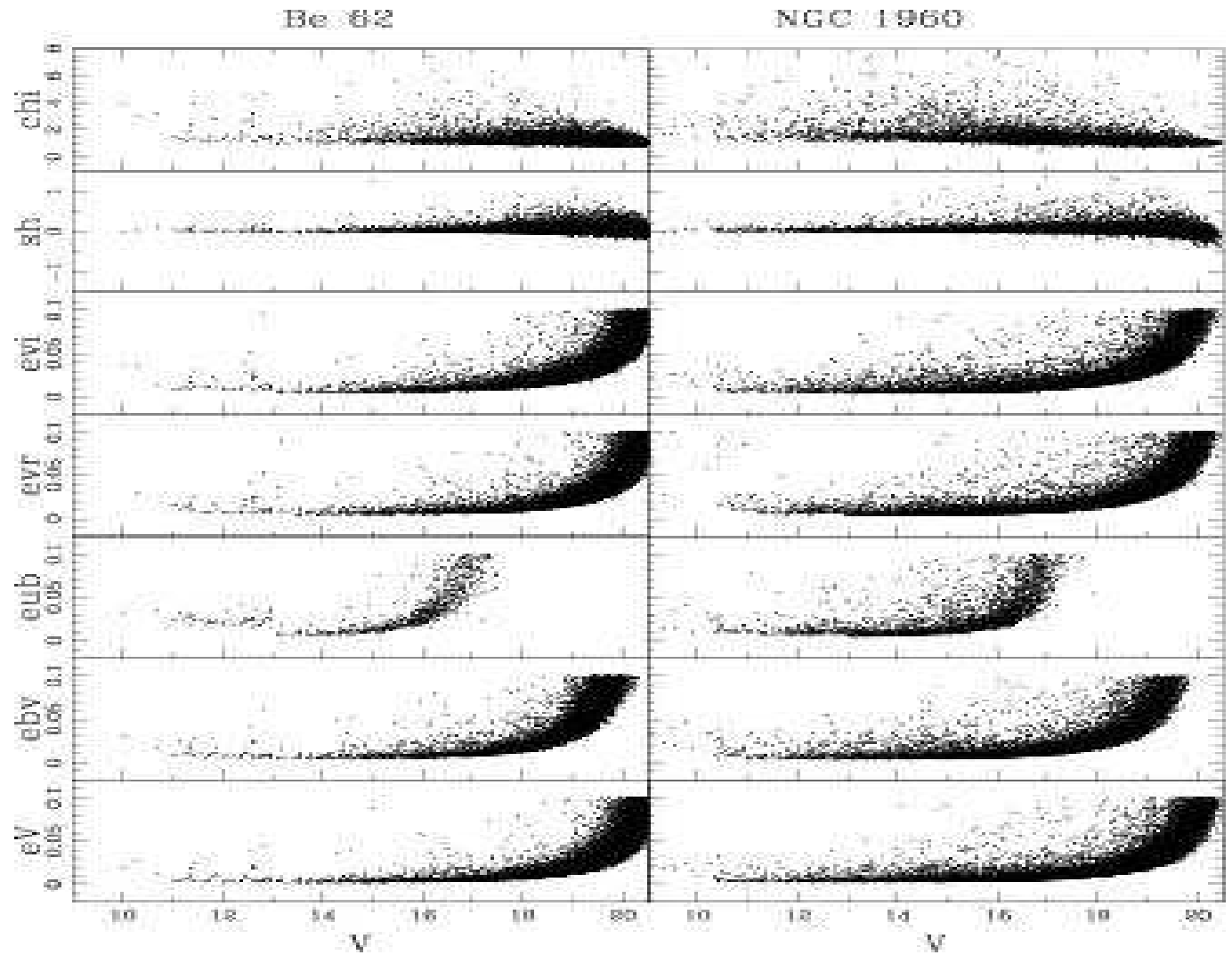


Fig. 2.— The DAOPHOT errors, image parameter χ and sharpness as a function of V magnitude for the measurements in the case of Be 62 and NGC 1960.

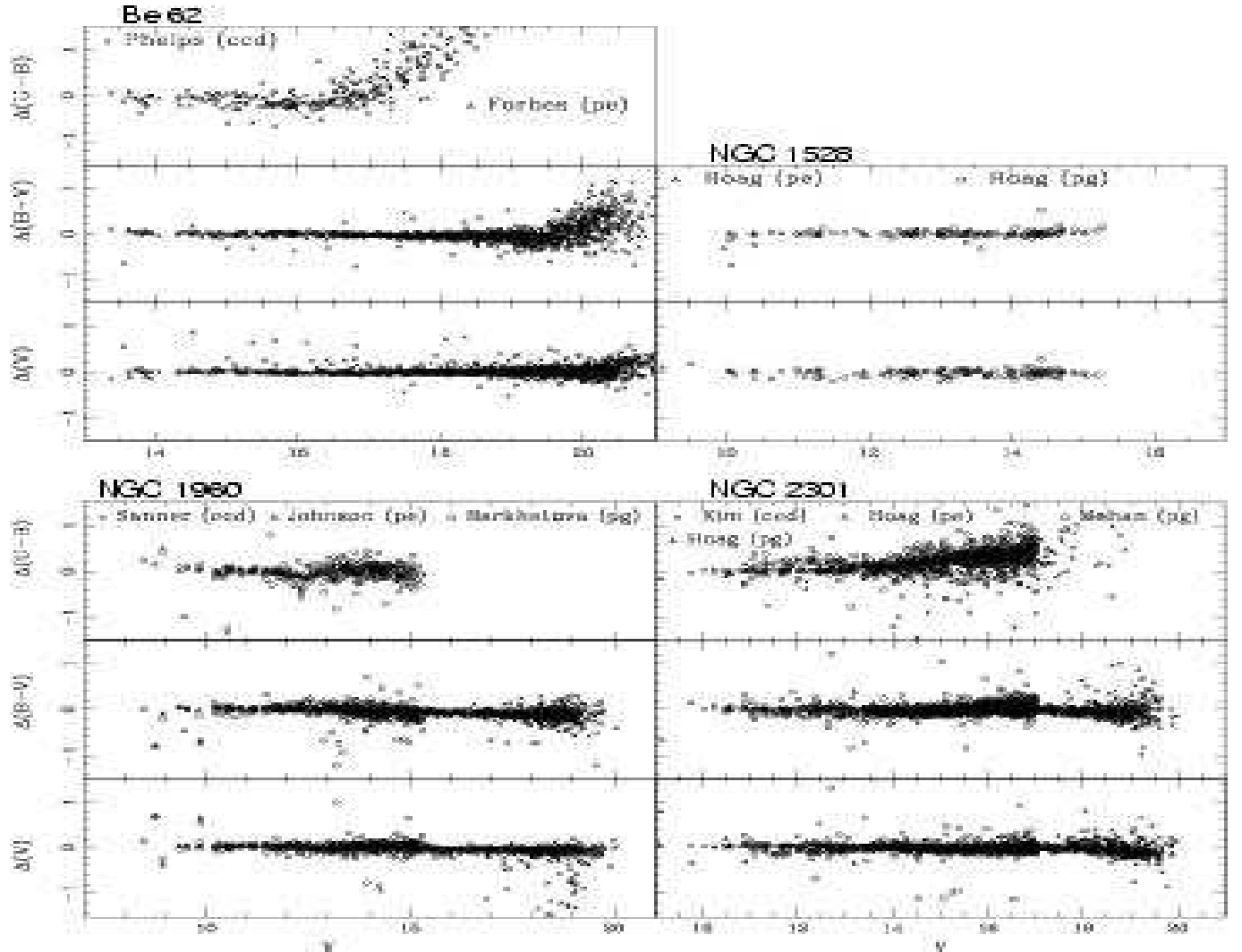


Fig. 3.— Comparison of the present CCD photometry with the data available in the literature. The difference Δ (literature - present data) as a function of V mag for all the target clusters is shown in figure. In the figure pe, pg, ccd indicate for photoelectric, photographic and CCD photometry respectively.

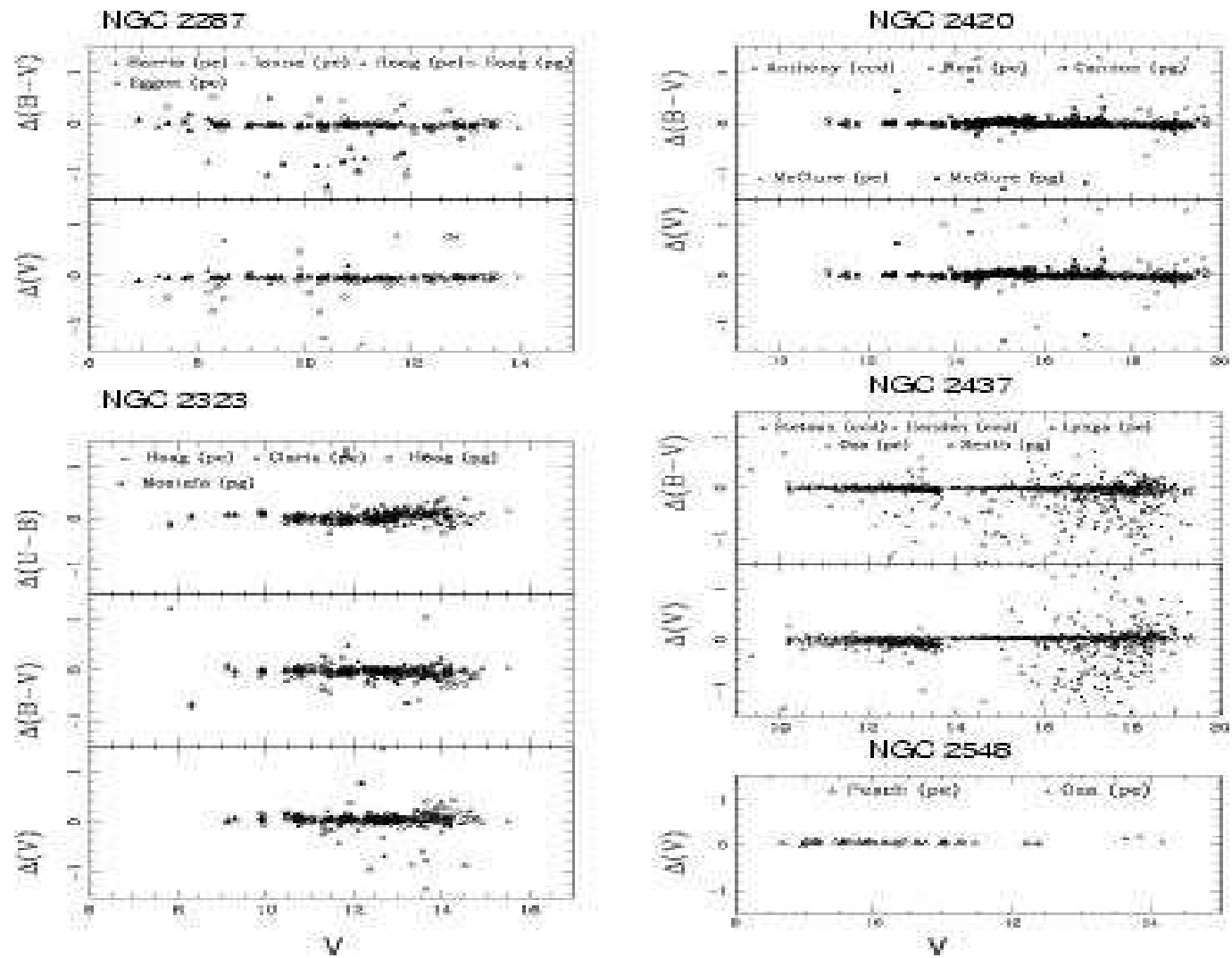


Fig. 3.— Continued

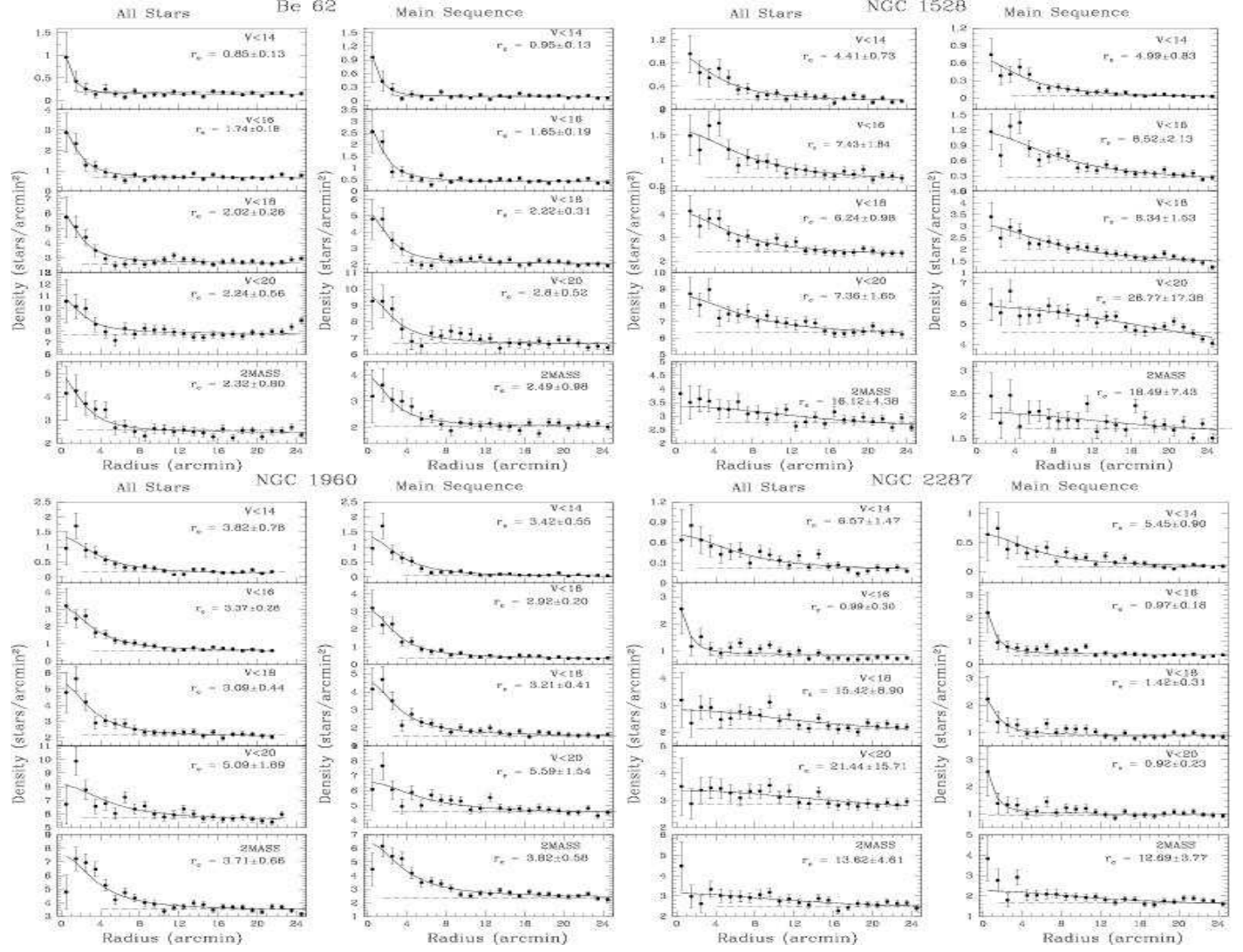


Fig. 4.— Radial density profile of clusters Be 62, NGC 1528, NGC 1960 and NGC 2287 for different magnitude levels using present optical and 2MASS data. Solid curve shows a least square fit of the King (1962) profile to the observed data points (see text). The error bars represent $\frac{1}{\sqrt{(N)}}$ errors. The dashed line indicates the density of field stars.

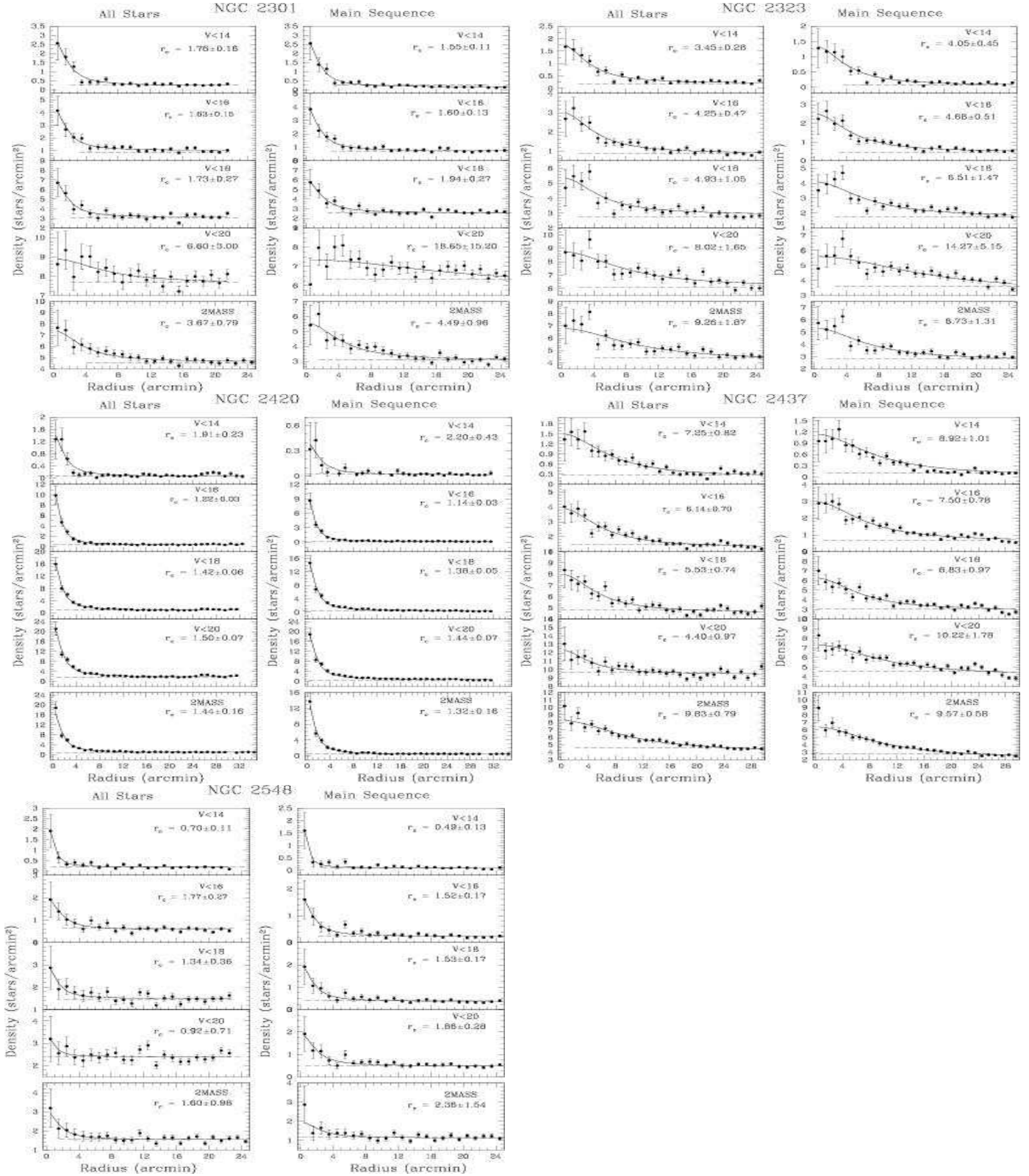


Fig. 4.— Continued for clusters NGC 2301, NGC 2323, NGC 2420, NGC 2437 and NGC 2548

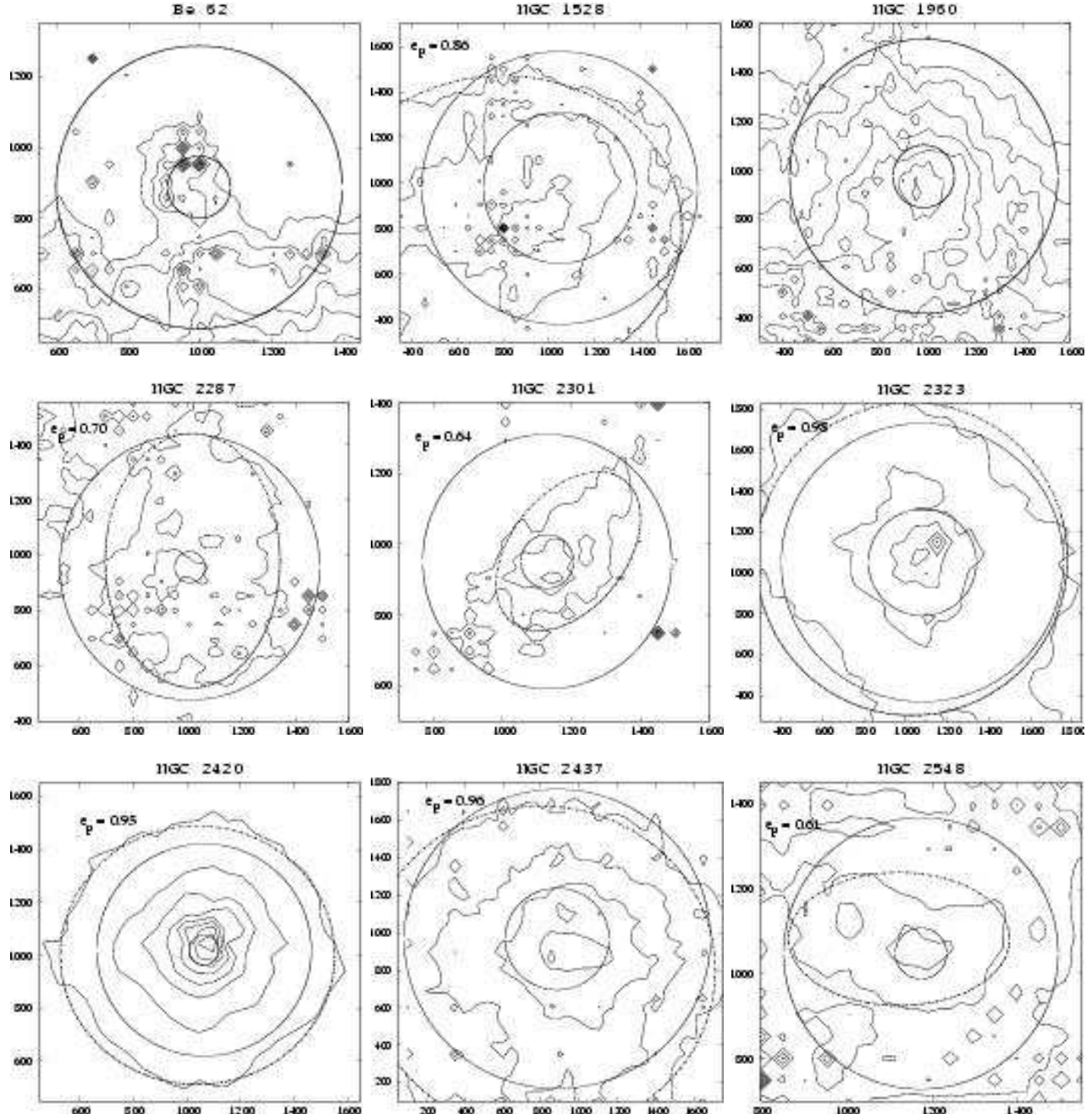


Fig. 5.— Isodensity contours drawn for the target clusters. The X and Y axis are in pixels. The inner and outer circles represent the core and cluster radius as obtained in the present study. Dashed curve shows the least square fitted curve to the outer region of the clusters. e_p is the elongation parameter (see text).

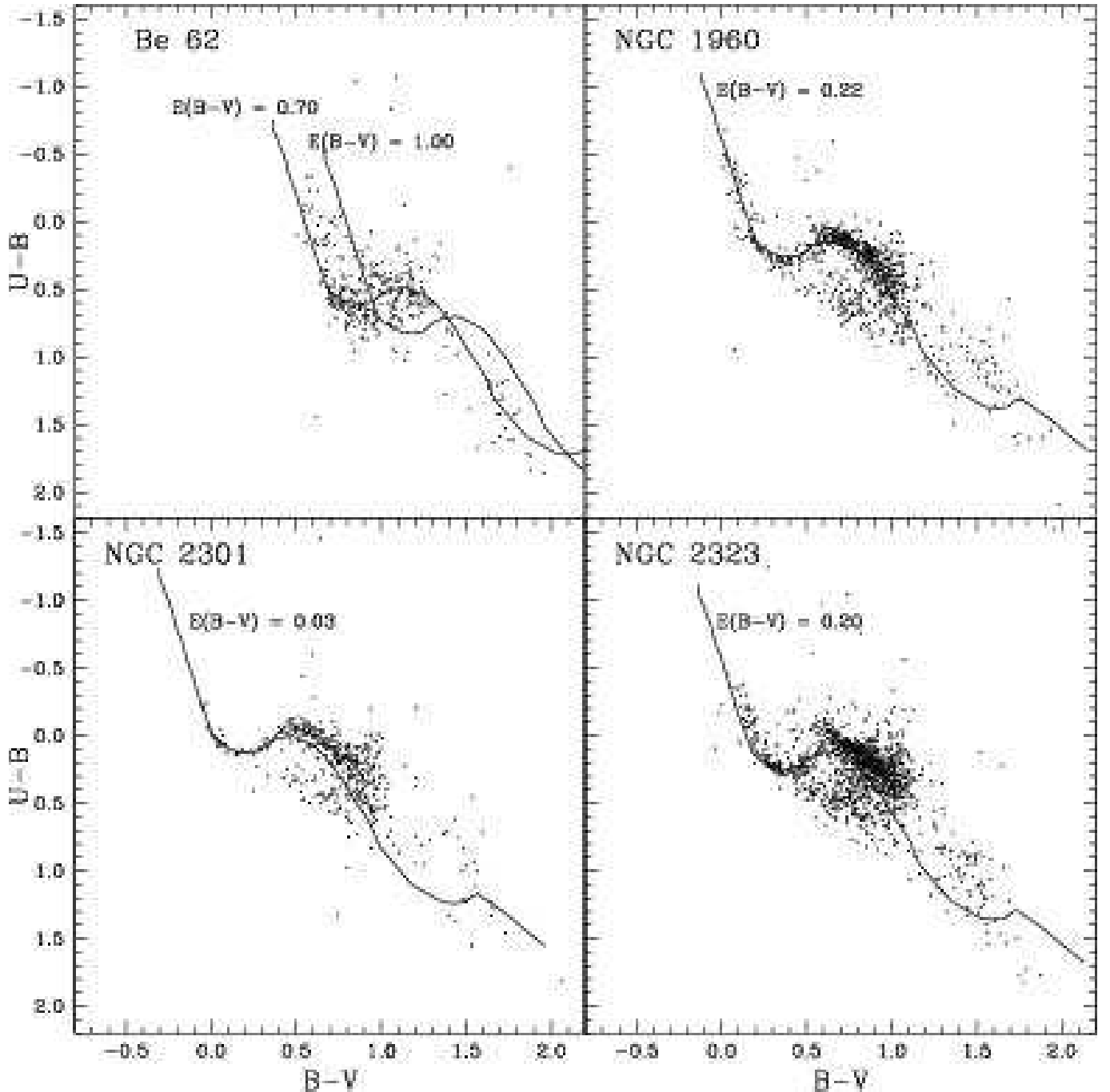


Fig. 6.— The $(U - B)/(B - V)$ color-color diagram for the stars within the region $r \leq r_{cl}$ of clusters Be 62, NGC 1960, NGC 2301 and NGC 2323. The continuous curve represents intrinsic MS for $Z = 0.02$ by Schmidt-Kaler (1982) shifted along the reddening vector of 0.72.

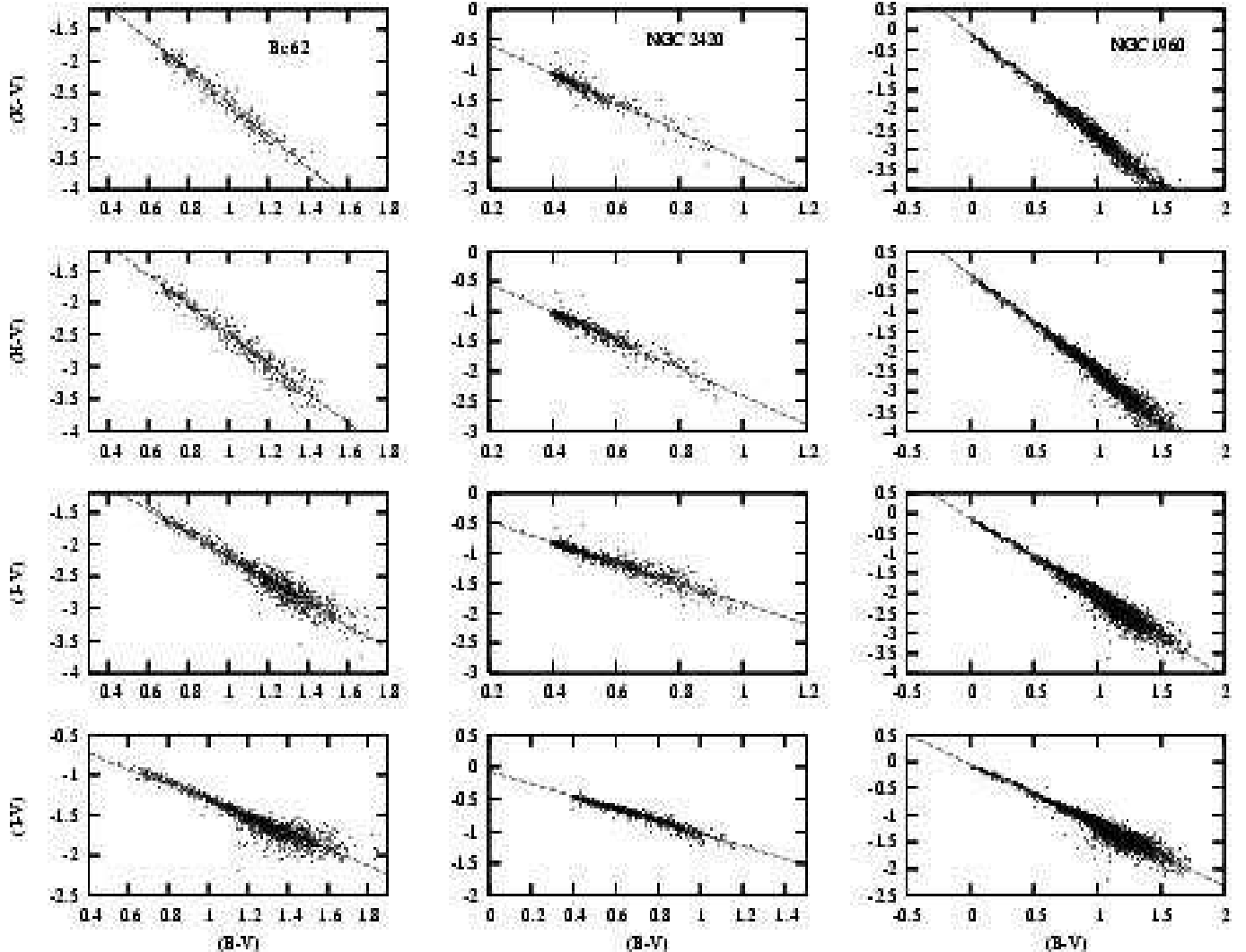


Fig. 7.— $(I - V)$, $(J - V)$, $(H - V)$, $(K - V)$ vs. $(B - V)$ two color diagrams, within the cluster region ($r \leq r_{cl}$), for the clusters Be 62, NGC 2420 and NGC 1960. Straight line shows a least square fit to the data.

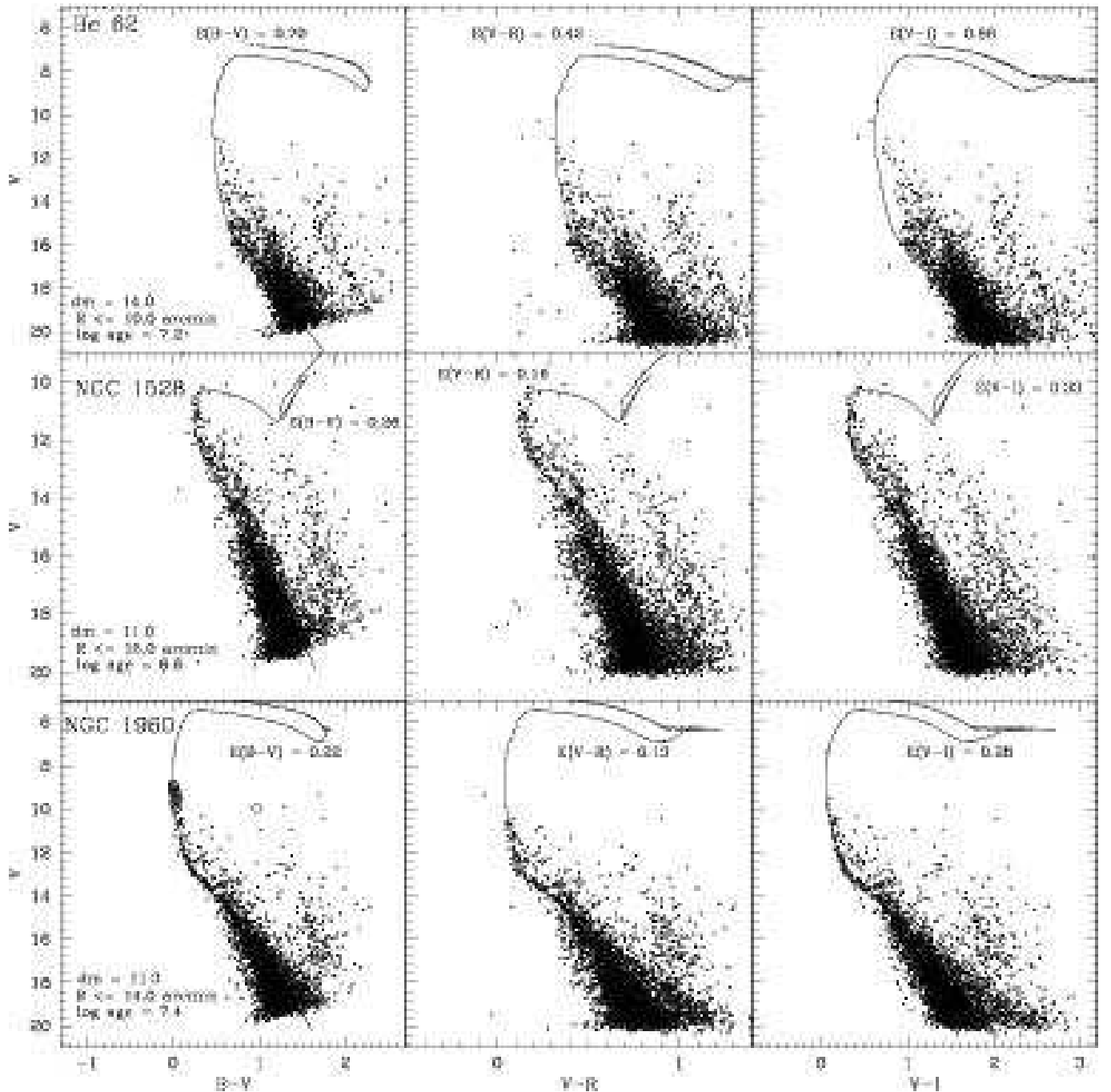


Fig. 8.— The V vs. $(B-V)$, $(V-R)$, $(V-I)$ CMDs for clusters Be 62, NGC 1528 and NGC 1960. The isochrones by Bertelli et al. (1994) for solar metallicity and indicated logarithmic age are also shown. The open circle represents photoelectric data taken from literature.

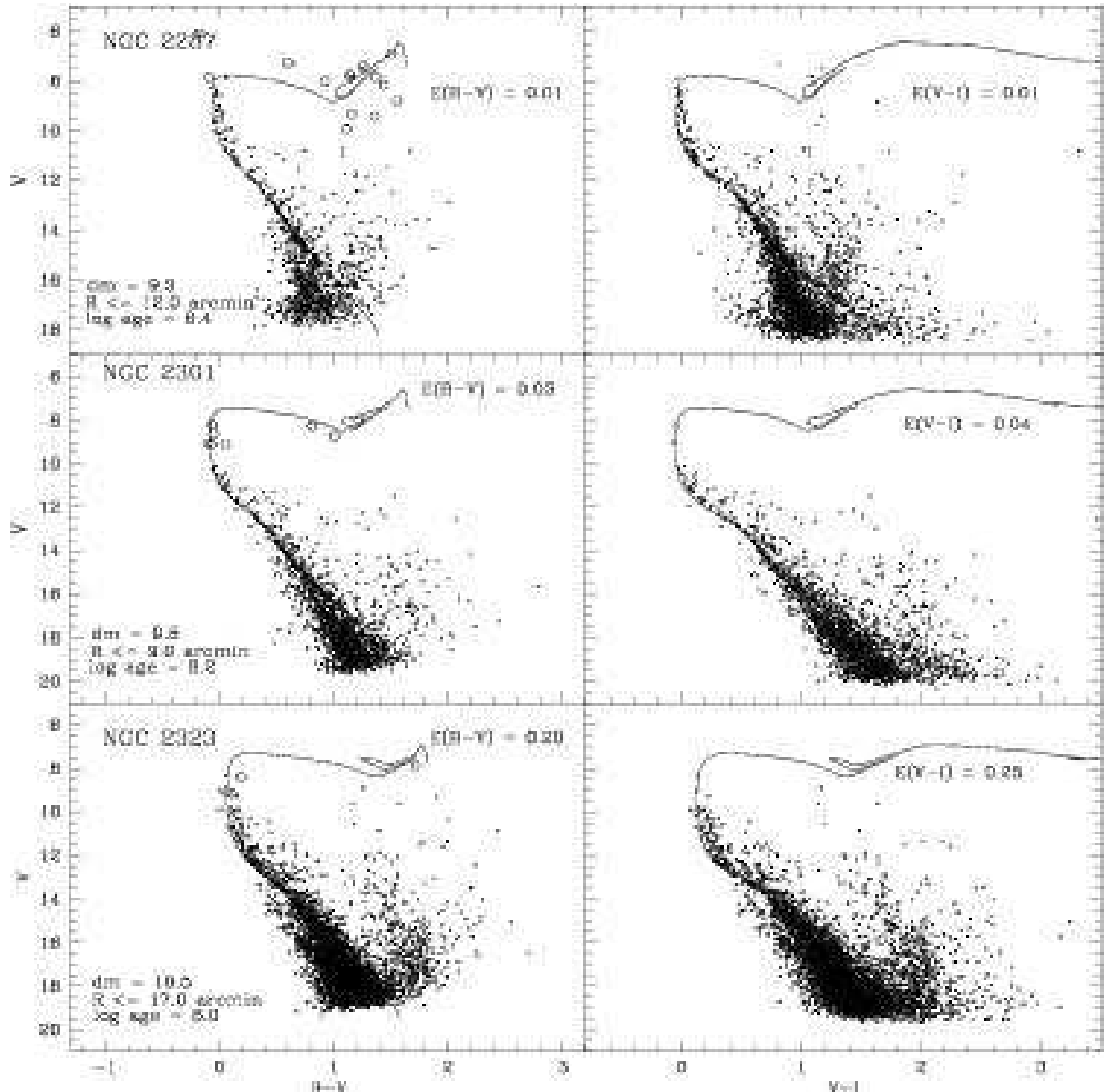


Fig. 8.— Continued - The V vs. $(B-V)$, $(V-I)$ CMDs for clusters NGC 2323, NGC 2301 and NGC 2287.

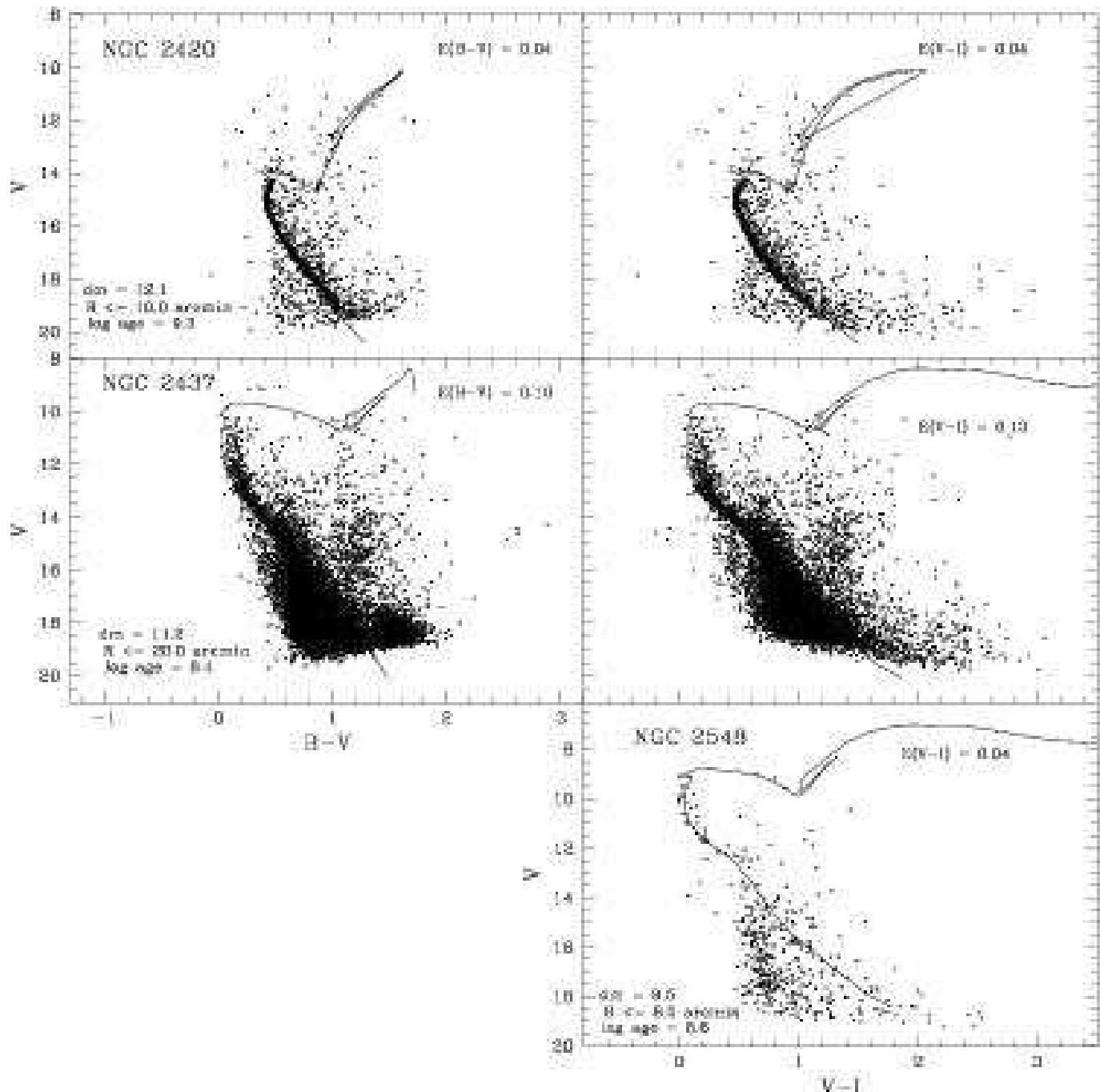


Fig. 8.— Continued - The V vs. $(B - V)$, $(V - I)$ CMDs for clusters NGC 2420, NGC 2437 and NGC 2548.

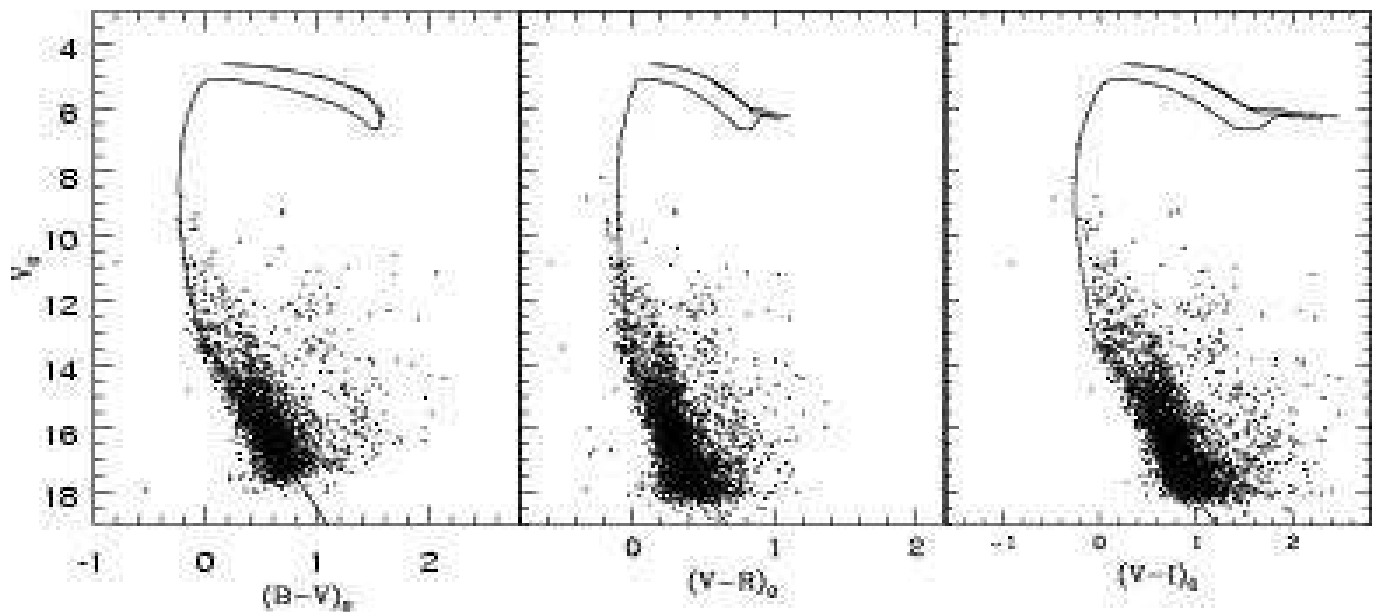


Fig. 9.— The unreddened CMDs for the cluster Be 62. The isochrone by Bertelli et al. (1994) for solar metallicity and log age = 7.2 is also shown.

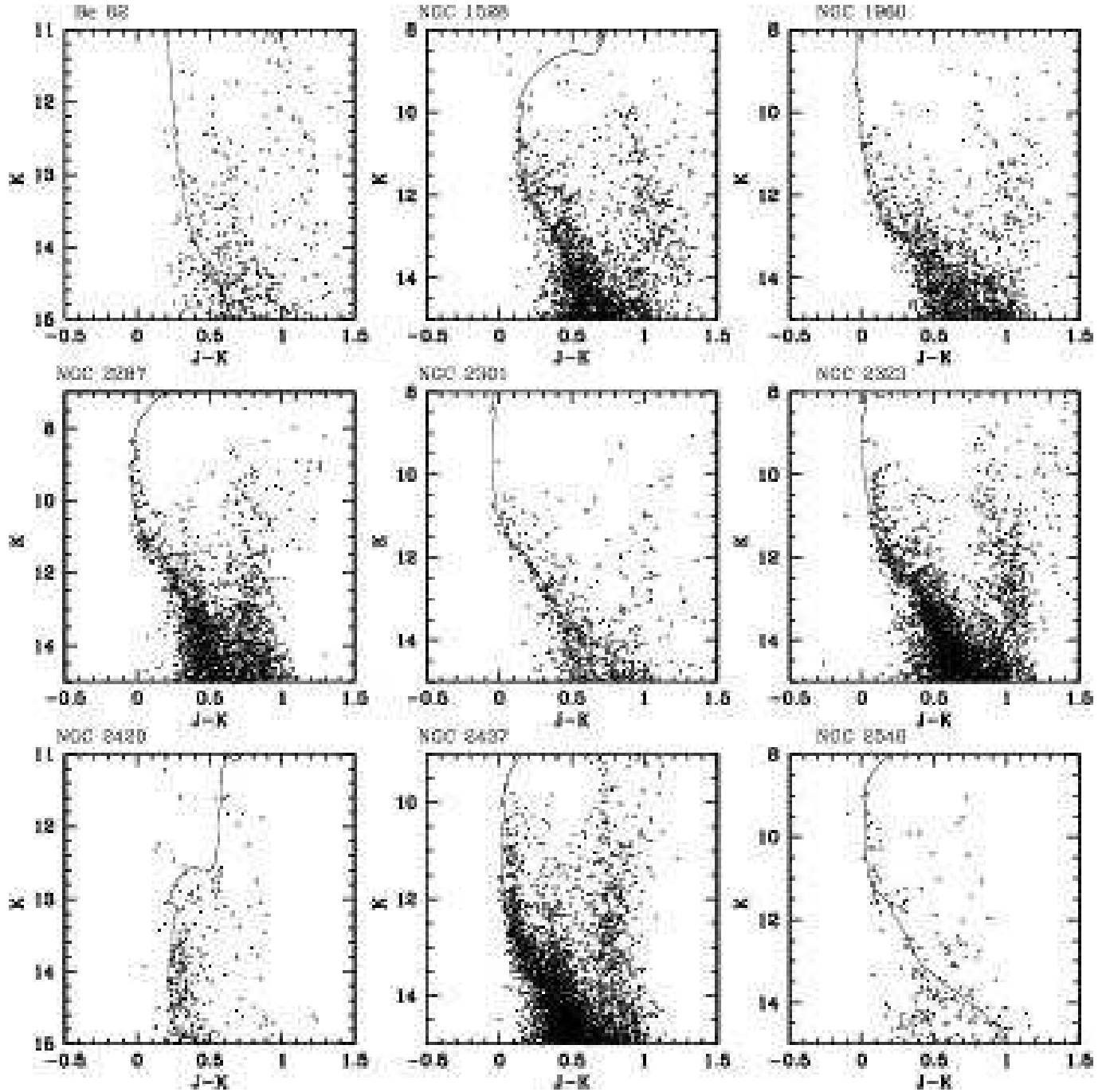


Fig. 10.— K vs. $(J - K)$ CMDs for target clusters obtained from 2MASS data. The isochrones by Bertelli et al. (1994) for the age obtained in the present work (cf. Table 8) are also shown. The values of $E(B - V)$ and distance modulus for the clusters has been adopted from Table 8.

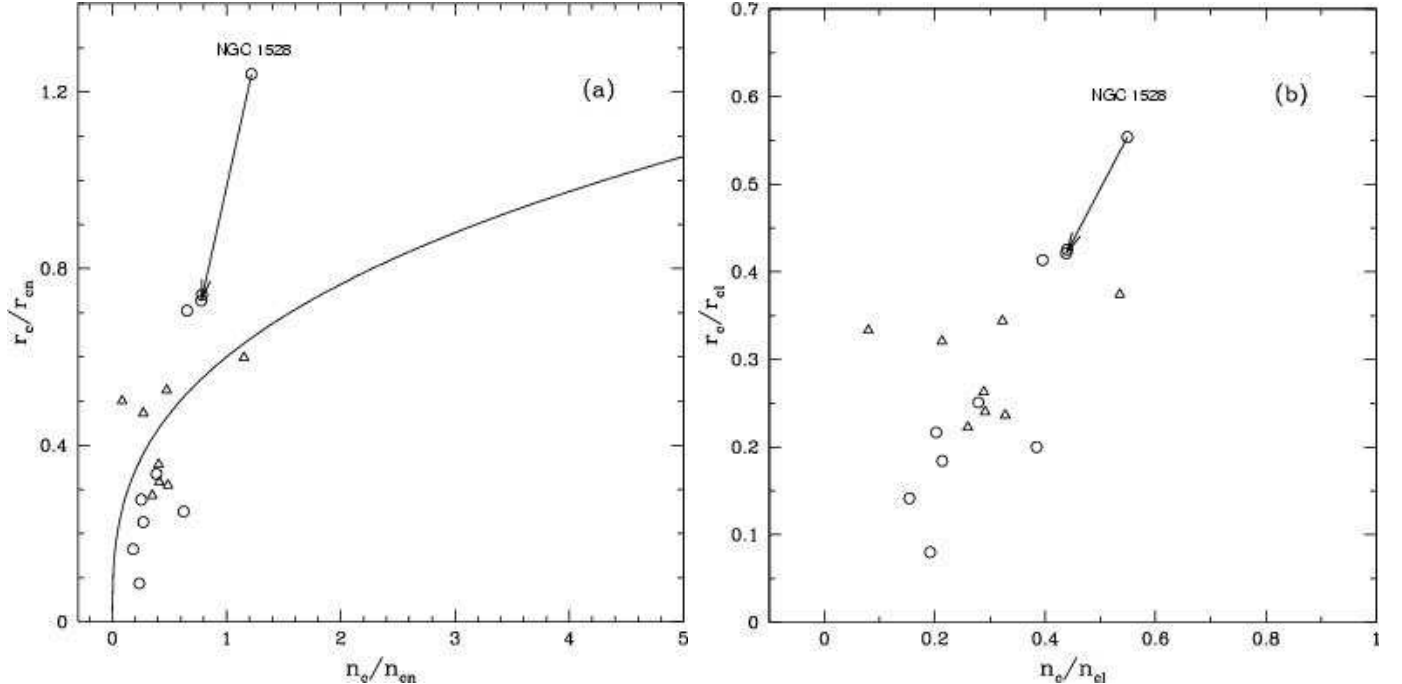


Fig. 11.— (a) The r_c/r_{cn} and n_c/n_{cn} diagram and (b) the r_c/r_{cl} and n_c/n_{cl} diagram for the clusters. Circles and triangle represent data taken from present study and previous studies respectively. The r_c , r_{cn} ($=r_{cl} - r_c$) and r_{cl} represents core radius, corona size and cluster extent respectively and n_c , n_{cn} and n_{cl} represents number of stars in the core, corona and total number of stars in the cluster respectively. The continuous curve represents relation $(\frac{r_c}{r_{cn}}) \propto (\frac{n_c}{n_{cn}})^{0.35}$ (cf. § 6). Arrow indicates the revised location of NGC 1528 (see text).

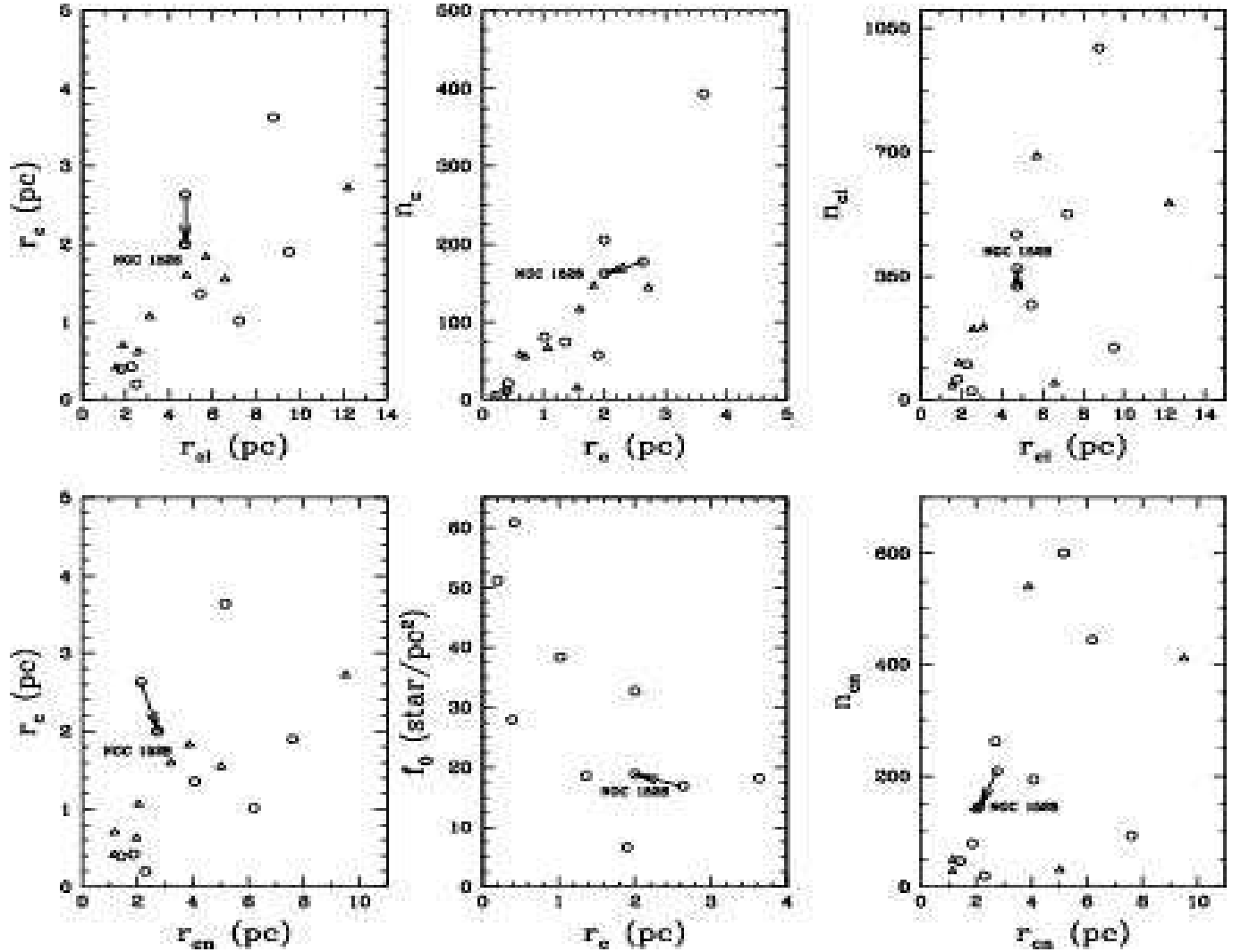


Fig. 12.— Correlation between various structural parameters of the clusters. Symbols are same as in Figure 11.

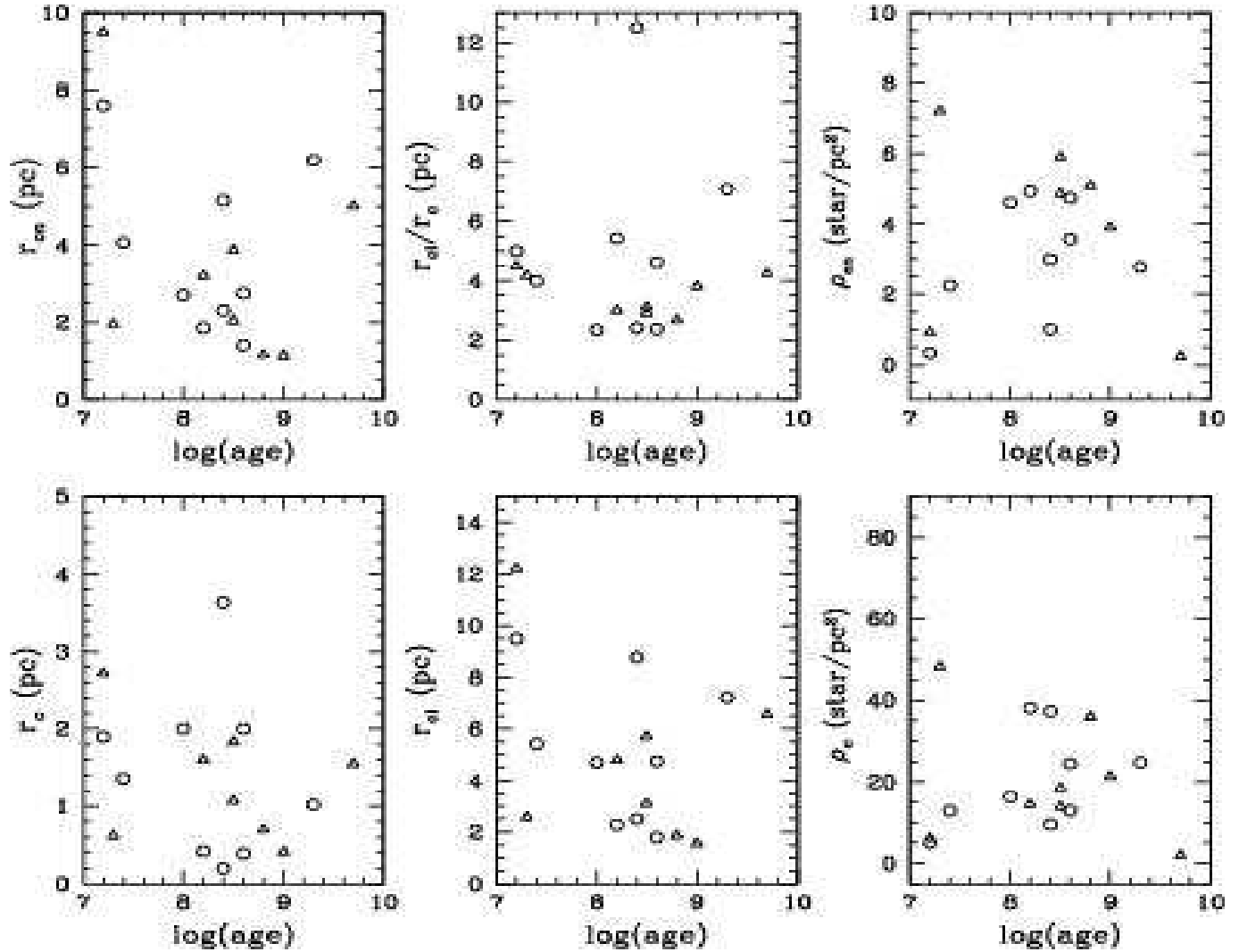


Fig. 13.— Various structural parameters of clusters as a function of age. Symbols are same as in Figure 11.

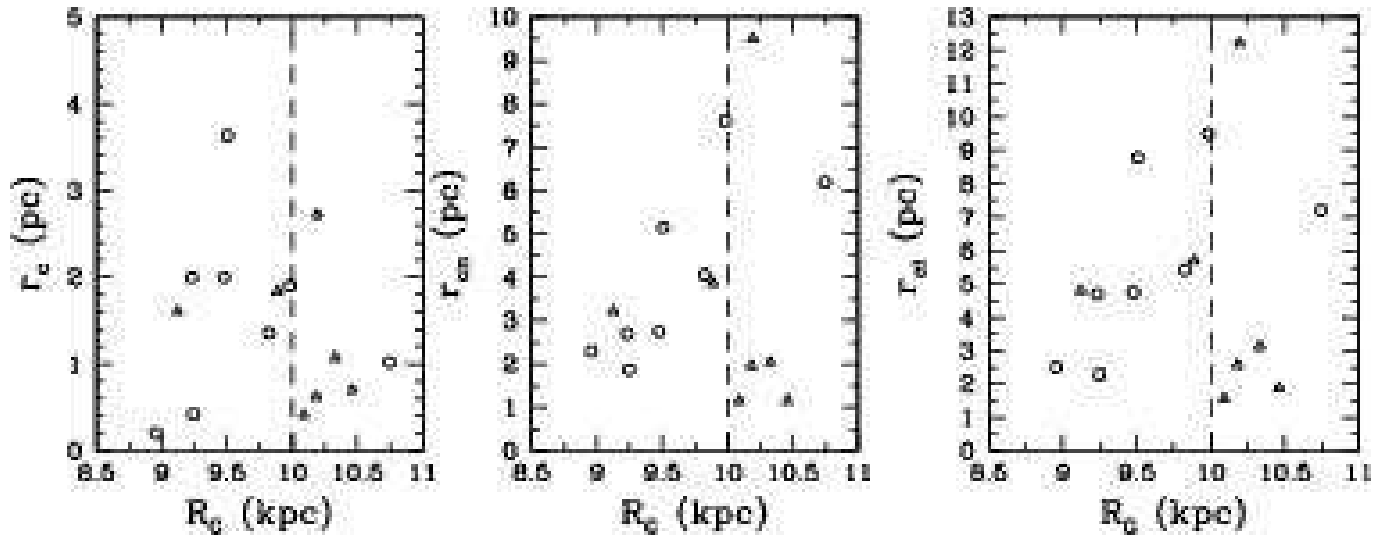


Fig. 14.— Dependence of cluster sizes on galactocentric distance ' R_G '. Symbols are same as in Figure 11. The r_c , r_{cn} and r_{cl} of the clusters located in $9 < R_G < 10$ kpc show an increasing trend with increasing R_G . The vertical dashed line is drawn to delineate the sample of clusters having $R_G < 10$ kpc and $R_G > 10$ kpc.

Table 1. Cluster parameters from WEBDA

Cluster	Cluster no. (IAU)	Trumpler class	α_{2000} (h:m:s)	δ_{2000} (d:m:s)	l (degree)	b (degree)	Log age (yr)	Distance (pc)	$E(B - V)$ (mag)
Be 62	C0057+636	III2m	01 : 01 : 00	63 : 57 : 00	123.98	1.10	7.2	1837	0.85
NGC 1528	C0411+511	II2m	04 : 15 : 23	51 : 12 : 54	152.06	0.26	8.6	776	0.26
NGC 1960	C0532+341	I3r	05 : 36 : 18	34 : 08 : 24	174.52	1.07	7.5	1318	0.22
NGC 2287	C0644-206	I3r	06 : 46 : 01	-20 : 45 : 24	231.02	-10.44	8.4	693	0.03
NGC 2301	C0649+005	I3r	06 : 51 : 45	00 : 27 : 36	212.56	0.28	8.2	872	0.03
NGC 2323	C0700-082	II3r	07 : 02 : 42	-08 : 23 : 00	221.67	-1.33	8.1	929	0.21
NGC 2420	C0735+216	I1r	07 : 38 : 23	21 : 34 : 24	198.11	19.63	9.1	3085	0.03
NGC 2437	C0739-147	II2r	07 : 41 : 46	-14 : 48 : 36	231.86	4.06	8.4	1375	0.15
NGC 2548	C0811-056	I3r	08 : 13 : 43	-05 : 45 : 00	227.87	15.39	8.6	769	0.03

Table 2. Log of Observations

Field	Filter	Exposure (seconds) \times No. of frames	Date
Be 62	<i>U</i>	180 \times 11, 60 \times 3	2001 Nov. 20
	<i>B</i>	90 \times 9, 30 \times 2, 20 \times 5	2001 Nov. 20
	<i>V</i>	90 \times 9, 20 \times 6	2001 Nov. 20
	<i>R</i>	60 \times 12, 10 \times 8	2001 Nov. 21
	<i>I</i>	60 \times 9, 20 \times 1, 10 \times 6	2001 Nov. 21
NGC 1528	<i>B</i>	60 \times 7, 10 \times 7	2001 Nov. 23
	<i>V</i>	60 \times 7, 10 \times 7	2001 Nov. 23
	<i>R</i>	60 \times 7, 10 \times 7, 5 \times 9	2001 Nov. 23
	<i>I</i>	60 \times 7, 10 \times 7, 5 \times 9	2001 Nov. 23
NGC 1960	<i>U</i>	180 \times 8, 30 \times 6	2001 Nov. 21
	<i>B</i>	60 \times 6, 20 \times 6, 10 \times 3	2001 Nov. 21
	<i>V</i>	60 \times 6, 30 \times 3, 10 \times 2	2001 Nov. 21
	<i>R</i>	30 \times 9, 10 \times 6	2001 Nov. 21
	<i>I</i>	30 \times 9, 10 \times 6, 5 \times 2	2001 Nov. 21
NGC 2287	<i>B</i>	60 \times 4, 10 \times 4, 5 \times 3	2001 Nov. 25
	<i>V</i>	60 \times 4, 10 \times 4, 5 \times 3	2001 Nov. 25
	<i>I</i>	60 \times 1, 30 \times 3, 10 \times 4, 5 \times 5	2001 Nov. 25
NGC 2301	<i>U</i>	180 \times 8, 60 \times 8	2001 Nov. 22
	<i>B</i>	60 \times 8, 20 \times 1, 10 \times 7	2001 Nov. 22
	<i>V</i>	60 \times 9, 10 \times 7	2001 Nov. 22
	<i>I</i>	60 \times 8, 10 \times 7	2001 Nov. 22
NGC 2323	<i>U</i>	180 \times 9, 60 \times 9	2001 Nov. 19
	<i>U</i>	180 \times 3	2001 Nov. 24
	<i>B</i>	60 \times 4, 10 \times 12	2001 Nov. 19
	<i>B</i>	60 \times 2	2001 Nov. 24
	<i>V</i>	60 \times 3, 10 \times 9	2001 Nov. 20
	<i>V</i>	60 \times 2	2001 Nov. 24
	<i>I</i>	30 \times 6, 10 \times 9	2001 Nov. 20
	<i>I</i>	10 \times 1	2001 Nov. 24
NGC 2420	<i>B</i>	60 \times 2, 10 \times 1	2001 Nov. 24
	<i>V</i>	60 \times 9, 20 \times 6, 10 \times 3	2001 Nov. 24
	<i>I</i>	60 \times 9, 10 \times 9	2001 Nov. 24
NGC 2437	<i>B</i>	60 \times 9, 20 \times 6	2001 Nov. 24
	<i>B</i>	60 \times 1, 20 \times 1	2001 Nov. 25
	<i>V</i>	60 \times 9, 20 \times 6, 10 \times 3	2001 Nov. 24
	<i>V</i>	60 \times 1, 20 \times 1	2001 Nov. 25
	<i>I</i>	60 \times 6, 30 \times 3, 10 \times 3	2001 Nov. 25
NGC 2548	<i>V</i>	60 \times 6, 10 \times 6	2001 Nov. 25
	<i>I</i>	60 \times 4, 10 \times 4, 5 \times 2	2001 Nov. 25

Table 3. The zero-point constants, color coefficients and extinction coefficients on different nights

Parameters	Date			
	2001 Nov. 22	2001 Nov. 23	2001 Nov. 24	2001 Nov. 25
Zero-point constant				
c_1	6.305 ± 0.005		6.189 ± 0.011	
c_2	2.553 ± 0.005	2.562 ± 0.003	2.488 ± 0.003	2.920 ± 0.006
c_3	2.882 ± 0.005	2.893 ± 0.004	2.841 ± 0.004	3.198 ± 0.008
c_4	2.564 ± 0.006	2.567 ± 0.004	2.531 ± 0.005	
c_5	3.545 ± 0.007	3.532 ± 0.007	3.491 ± 0.005	3.762 ± 0.010
Color coefficient				
m_1	-0.045 ± 0.008		-0.014 ± 0.010	
m_2	-0.116 ± 0.004	-0.125 ± 0.003	-0.112 ± 0.003	-0.136 ± 0.006
m_3	0.068 ± 0.005	0.068 ± 0.004	0.070 ± 0.003	0.067 ± 0.006
m_4	0.031 ± 0.009	0.040 ± 0.007	0.047 ± 0.007	
m_5	-0.076 ± 0.006	-0.076 ± 0.006	-0.061 ± 0.004	-0.083 ± 0.008
Extinction coefficient				
k_u	0.661 ± 0.028		0.683 ± 0.028	
k_b	0.261 ± 0.012	0.352 ± 0.007	0.295 ± 0.007	0.211 ± 0.012
k_v	0.176 ± 0.010	0.218 ± 0.012	0.183 ± 0.008	0.133 ± 0.015
k_r	0.150 ± 0.009	0.181 ± 0.012	0.128 ± 0.010	
k_i	0.047 ± 0.009	0.140 ± 0.021	0.096 ± 0.010	0.037 ± 0.020

Table 4. Comparison of the present photometry with the available photometry in the literature. The difference Δ (literature-present data) is in magnitude. Mean and σ are based on N stars in a V magnitude bin.

V range	$\Delta(V)$ (Mean $\pm \sigma$)	(N)	$\Delta(B - V)$ (Mean $\pm \sigma$)	(N)	$\Delta(U - B)$ (Mean $\pm \sigma$)	(N)
Be 62						
Phelps & Janes (1994, ccd)						
13-14	0.010 \pm 0.033	9	0.022 \pm 0.023	9	-0.112 \pm 0.123	9
14-15	0.021 \pm 0.066	30	-0.021 \pm 0.068	30	-0.073 \pm 0.106	27
15-16	0.002 \pm 0.053	65	-0.005 \pm 0.057	65	-0.129 \pm 0.126	57
16-17	-0.002 \pm 0.063	92	-0.017 \pm 0.052	92	-0.023 \pm 0.223	74
17-18	-0.002 \pm 0.057	165	-0.045 \pm 0.060	165	0.394 \pm 0.321	64
18-19	0.007 \pm 0.070	239	-0.064 \pm 0.087	239	1.227 \pm 0.420	30
19-20	0.010 \pm 0.089	328	-0.022 \pm 0.193	315	1.480 \pm 0.000	1
20-21	0.043 \pm 0.149	285	0.267 \pm 0.318	199		
Forbes (1981, pe)						
13-14	-0.129 \pm 0.024	4	0.062 \pm 0.030	4	-0.014 \pm 0.122	4
NGC 1528						
Hoag et al. (1961, pe)						
<11	0.024 \pm 0.031	6	0.001 \pm 0.014	5		
11-12	0.011 \pm 0.008	4	-0.006 \pm 0.006	4		
12-13	-0.001 \pm 0.015	5	-0.006 \pm 0.008	5		
13-14	0.014 \pm 0.017	5	-0.006 \pm 0.011	5		
14-15	-0.011 \pm 0.010	5	0.013 \pm 0.037	5		
Hoag et al. (1961, pg)						
<11	-0.011 \pm 0.115	7	-0.067 \pm 0.102	6		
11-12	-0.079 \pm 0.066	12	0.021 \pm 0.048	12		
12-13	-0.034 \pm 0.066	23	0.010 \pm 0.043	23		
13-14	-0.024 \pm 0.066	30	-0.005 \pm 0.056	30		
14-15	-0.023 \pm 0.080	38	0.028 \pm 0.099	38		
15-16	-0.064 \pm 0.023	3	0.046 \pm 0.022	3		
NGC 1960						
Sanmer et al. (2000, ccd)						
<10	0.008 \pm 0.028	3	-0.033 \pm 0.058	3		
10-11	-0.009 \pm 0.016	10	0.035 \pm 0.022	10		
11-12	-0.005 \pm 0.015	15	0.019 \pm 0.013	15		
12-13	-0.006 \pm 0.016	25	-0.007 \pm 0.033	25		
13-14	-0.001 \pm 0.050	33	-0.002 \pm 0.034	33		
14-15	-0.001 \pm 0.092	24	-0.014 \pm 0.053	24		
15-16	-0.040 \pm 0.054	91	-0.060 \pm 0.053	91		
16-17	-0.046 \pm 0.048	99	-0.079 \pm 0.044	99		
17-18	-0.057 \pm 0.065	148	-0.105 \pm 0.077	148		
18-19	-0.058 \pm 0.068	268	-0.123 \pm 0.127	265		
19-20	-0.080 \pm 0.103	75	-0.132 \pm 0.178	62		
Johnson & Morgan (1953, pe)						
<10	-0.014 \pm 0.067	6	-0.024 \pm 0.053	5	0.169 \pm 0.214	5
10-11	0.019 \pm 0.009	11	0.009 \pm 0.011	11	-0.005 \pm 0.043	10
11-12	0.016 \pm 0.016	16	-0.003 \pm 0.013	16	-0.012 \pm 0.048	15
12-13	0.003 \pm 0.025	4	0.001 \pm 0.008	4	-0.221 \pm 0.228	4

Table 4—Continued

V range	$\Delta(V)$ (Mean \pm σ)	(N)	$\Delta(B - V)$ (Mean \pm σ)	(N)	$\Delta(U - B)$ (Mean \pm σ)	(N)
Barkhatova et al. (1984, pg)						
< 10	-0.032 \pm 0.129	5	-0.076 \pm 0.124	4	0.171 \pm 0.164	4
10-11	0.018 \pm 0.054	18	-0.010 \pm 0.085	18	-0.010 \pm 0.078	16
11-12	0.027 \pm 0.065	27	0.026 \pm 0.078	27	-0.027 \pm 0.099	27
12-13	-0.008 \pm 0.074	52	0.046 \pm 0.080	51	-0.088 \pm 0.141	50
13-14	0.002 \pm 0.080	99	-0.005 \pm 0.134	98	0.033 \pm 0.159	86
14-15	0.023 \pm 0.080	118	-0.058 \pm 0.114	117	0.003 \pm 0.131	90
15-16	0.043 \pm 0.073	34	-0.148 \pm 0.102	33	-0.075 \pm 0.191	17
NGC 2287						
Harris et al. (1993, pe)						
< 8	-0.061 \pm 0.032	5	-0.032 \pm 0.084	5		
8-9	-0.054 \pm 0.009	7	-0.031 \pm 0.014	7		
9-10	-0.058 \pm 0.048	10	-0.032 \pm 0.006	9		
10-11	-0.047 \pm 0.059	16	-0.026 \pm 0.029	16		
11-12	-0.056 \pm 0.017	10	-0.029 \pm 0.019	10		
12-13	-0.055 \pm 0.015	7	-0.040 \pm 0.022	7		
13-14	-0.058 \pm 0.010	3	-0.045 \pm 0.019	3		
Eggen (1974, pe)						
<8	-0.065 \pm 0.041	4	-0.008 \pm 0.092	4		
8-9	-0.014 \pm 0.045	8	-0.010 \pm 0.043	8		
9-10	-0.025 \pm 0.009	3	-0.043 \pm 0.003	3		
10-11	-0.024 \pm 0.017	5	-0.021 \pm 0.012	4		
11-12	-0.049 \pm 0.028	2	-0.030 \pm 0.037	2		
12-13	-0.022 \pm 0.010	2	-0.050 \pm 0.003	2		
13-14	-0.049 \pm 0.000	1	-0.042 \pm 0.000	1		
Ianna et al. (1987, pe)						
<8	-0.061 \pm 0.030	5	-0.032 \pm 0.073	5		
8-9	-0.057 \pm 0.022	9	-0.038 \pm 0.035	9		
9-10	-0.025 \pm 0.064	9	-0.031 \pm 0.012	9		
10-11	-0.042 \pm 0.055	24	-0.025 \pm 0.020	24		
11-12	-0.059 \pm 0.025	16	-0.024 \pm 0.018	16		
Hoag et al. (1961, pe)						
<8	-0.076 \pm 0.000	1	0.075 \pm 0.000	1		
8-9	-0.136 \pm 0.179	3	-0.024 \pm 0.090	3		
9-10	-0.045 \pm 0.015	2	-0.031 \pm 0.040	2		
10-11	-0.035 \pm 0.017	6	-0.056 \pm 0.040	6		
12-13	-0.032 \pm 0.020	3	-0.060 \pm 0.029	3		
13-14	-0.071 \pm 0.054	2	-0.039 \pm 0.086	2		
Hoag et al. (1961, pg)						
8-9	-0.120 \pm 0.015	3	-0.058 \pm 0.063	3		
9-10	-0.097 \pm 0.022	4	-0.050 \pm 0.023	3		
10-11	-0.111 \pm 0.106	9	-0.029 \pm 0.087	9		
11-12	-0.104 \pm 0.048	10	-0.037 \pm 0.036	10		
12-13	-0.055 \pm 0.043	17	-0.075 \pm 0.054	17		
13-14	-0.038 \pm 0.038	9	-0.012 \pm 0.038	9		

Table 4—Continued

V range	$\Delta(V)$ (Mean $\pm \sigma$)	(N)	$\Delta(B - V)$ (Mean $\pm \sigma$)	(N)	$\Delta(U - B)$ (Mean $\pm \sigma$)	(N)
NGC 2301						
Kim et al. (2001, ccd)						
10-11	0.021 \pm 0.016	11	0.014 \pm 0.016	11	0.002 \pm 0.022	11
11-12	0.043 \pm 0.054	18	0.002 \pm 0.019	18	-0.030 \pm 0.191	18
12-13	0.026 \pm 0.057	27	-0.002 \pm 0.035	27	0.005 \pm 0.069	23
13-14	0.020 \pm 0.021	21	0.013 \pm 0.020	21	-0.027 \pm 0.085	21
14-15	0.014 \pm 0.080	55	0.003 \pm 0.055	55	-0.047 \pm 0.113	42
15-16	0.015 \pm 0.049	67	-0.001 \pm 0.049	67	-0.010 \pm 0.186	61
16-17	0.016 \pm 0.083	98	0.002 \pm 0.077	98	0.096 \pm 0.244	73
17-18	0.001 \pm 0.068	157	-0.031 \pm 0.069	152	0.374 \pm 0.337	33
18-19	-0.028 \pm 0.106	255	-0.062 \pm 0.116	247	0.539 \pm 0.652	9
19-20	-0.082 \pm 0.130	128	-0.053 \pm 0.208	105		
Hoag et al. (1961, pe)						
10-11	0.052 \pm 0.031	3	-0.011 \pm 0.022	3	-0.027 \pm 0.015	2
11-12	0.038 \pm 0.011	8	0.006 \pm 0.013	8	0.001 \pm 0.058	8
12-13	0.031 \pm 0.010	7	0.017 \pm 0.020	7	0.011 \pm 0.047	7
13-14	0.004 \pm 0.029	4	0.026 \pm 0.018	4	0.090 \pm 0.015	4
Mohan & Sagar (1988, pg)						
11-12	-0.043 \pm 0.088	26	-0.050 \pm 0.099	26	0.125 \pm 0.146	23
12-13	-0.026 \pm 0.086	44	-0.043 \pm 0.122	44	0.132 \pm 0.145	37
13-14	0.005 \pm 0.062	69	-0.075 \pm 0.086	68	0.106 \pm 0.108	66
14-15	-0.011 \pm 0.057	153	-0.045 \pm 0.073	153	0.209 \pm 0.191	140
15-16	-0.038 \pm 0.055	220	0.011 \pm 0.119	220	0.297 \pm 0.129	196
16-17	-0.018 \pm 0.068	335	0.047 \pm 0.108	335	0.397 \pm 0.187	247
Hoag et al. (1961, pg)						
10-11	-0.019 \pm 0.211	4	0.045 \pm 0.075	4	0.003 \pm 0.118	4
11-12	0.054 \pm 0.000	1	-0.010 \pm 0.000	1	-0.023 \pm 0.000	1
12-13	-0.029 \pm 0.117	11	0.058 \pm 0.068	11	0.032 \pm 0.170	10
13-14	-0.044 \pm 0.098	13	0.069 \pm 0.100	13	0.097 \pm 0.088	12
14-15	0.019 \pm 0.050	8	0.038 \pm 0.038	8	0.166 \pm 0.076	6
NGC 2323						
Hoag et al. (1961, pe)						
<10	0.058 \pm 0.029	6	-0.007 \pm 0.054	6	0.078 \pm 0.036	6
11-12	0.058 \pm 0.000	1	-0.006 \pm 0.000	1	0.056 \pm 0.000	1
12-13	0.052 \pm 0.019	5	-0.024 \pm 0.031	5	0.018 \pm 0.062	5
13-14	0.106 \pm 0.074	2	-0.081 \pm 0.066	2	0.061 \pm 0.007	2
14-15	0.053 \pm 0.039	3	-0.070 \pm 0.015	3	0.102 \pm 0.118	2
15-16	0.017 \pm 0.000	1	0.051 \pm 0.000	1	0.157 \pm 0.000	1
Claria et al. (1988, pe)						
<10	0.038 \pm 0.033	6	0.009 \pm 0.049	6	0.074 \pm 0.023	6
10-11	0.046 \pm 0.010	12	-0.007 \pm 0.015	12	0.045 \pm 0.023	12
11-12	0.051 \pm 0.017	23	-0.013 \pm 0.018	23	0.000 \pm 0.040	22
12-13	0.023 \pm 0.067	33	-0.002 \pm 0.022	33	0.012 \pm 0.047	33
13-14	0.011 \pm 0.037	10	0.016 \pm 0.025	10	0.025 \pm 0.072	9
14-15	-0.007 \pm 0.037	2	-0.001 \pm 0.042	2	0.062 \pm 0.059	2

Table 4—Continued

V range	$\Delta(V)$ (Mean $\pm \sigma$)	(N)	$\Delta(B - V)$ (Mean $\pm \sigma$)	(N)	$\Delta(U - B)$ (Mean $\pm \sigma$)	(N)
Hoag et al. (1961, pg)						
<11	0.092 \pm 0.063	11	0.001 \pm 0.06	11	-0.030 \pm 0.055	11
11-12	0.049 \pm 0.094	24	-0.018 \pm 0.078	22	-0.041 \pm 0.050	22
12-13	0.052 \pm 0.044	36	-0.030 \pm 0.050	35	-0.001 \pm 0.096	35
13-14	0.111 \pm 0.087	28	-0.072 \pm 0.075	28	-0.105 \pm 0.054	25
14-15	0.104 \pm 0.074	13	-0.143 \pm 0.111	13	0.028 \pm 0.195	10
Mostafa et al. (1983, pg)						
<10	0.079 \pm 0.095	5	-0.045 \pm 0.069	5	0.094 \pm 0.037	5
10-11	0.058 \pm 0.075	9	-0.048 \pm 0.097	9	-0.004 \pm 0.032	9
11-12	0.027 \pm 0.117	17	0.006 \pm 0.123	17	0.065 \pm 0.089	13
12-13	0.036 \pm 0.075	29	-0.072 \pm 0.103	28	0.049 \pm 0.090	28
13-14	0.035 \pm 0.113	22	-0.027 \pm 0.120	22	-0.019 \pm 0.015	21
14-15	0.002 \pm 0.082	12	-0.022 \pm 0.078	12	0.021 \pm 0.099	11
NGC 2420						
Anthony-Twarog et al. (1990, ccd)						
11-12	0.024 \pm 0.011	2	0.023 \pm 0.014	2		
12-13	0.011 \pm 0.015	8	-0.003 \pm 0.021	8		
13-14	0.014 \pm 0.027	11	-0.013 \pm 0.016	11		
14-15	0.002 \pm 0.017	55	-0.016 \pm 0.011	55		
15-16	-0.006 \pm 0.014	64	-0.013 \pm 0.015	64		
16-17	-0.006 \pm 0.040	78	-0.017 \pm 0.023	78		
17-18	-0.013 \pm 0.040	80	-0.017 \pm 0.026	79		
18-19	-0.027 \pm 0.076	110	-0.002 \pm 0.075	110		
19-20	-0.006 \pm 0.084	48	0.056 \pm 0.014	48		
West (1967, pe)						
11-12	0.013 \pm 0.037	5	0.010 \pm 0.011	5		
12-13	-0.004 \pm 0.012	8	0.021 \pm 0.073	8		
13-14	-0.010 \pm 0.005	3	-0.004 \pm 0.012	3		
14-15	-0.005 \pm 0.008	7	-0.007 \pm 0.034	7		
15-16	-0.014 \pm 0.012	6	-0.015 \pm 0.022	6		
17-18	0.002 \pm 0.017	2	-0.028 \pm 0.036	2		
Mc Clure et al. (1974, pe)						
11-12	0.009 \pm 0.019	5	0.011 \pm 0.011	5		
12-13	0.012 \pm 0.011	7	0.011 \pm 0.012	7		
13-14	0.006 \pm 0.006	4	-0.006 \pm 0.013	4		
14-15	0.015 \pm 0.009	5	-0.010 \pm 0.012	5		
15-16	0.015 \pm 0.000	1	0.023 \pm 0.000	1		
Mc Clure et al. (1974, pg)						
12-13	0.024 \pm 0.021	2	0.005 \pm 0.042	2		
13-14	0.027 \pm 0.043	10	0.004 \pm 0.018	10		
14-15	0.027 \pm 0.031	50	-0.008 \pm 0.019	50		
15-16	0.002 \pm 0.041	62	-0.012 \pm 0.027	62		
16-17	0.001 \pm 0.058	70	-0.003 \pm 0.040	70		
17-18	0.015 \pm 0.068	36	-0.017 \pm 0.041	35		
Cannon & Lloyd (1970, pg)						

Table 4—Continued

V range	$\Delta(V)$ (Mean \pm σ)	(N)	$\Delta(B - V)$ (Mean \pm σ)	(N)	$\Delta(U - B)$ (Mean \pm σ)	(N)
11-12	-0.015 ± 0.059	5	0.055 ± 0.075	5		
12-13	0.002 ± 0.016	11	0.021 ± 0.024	11		
13-14	-0.031 ± 0.036	21	0.031 ± 0.050	21		
14-15	-0.056 ± 0.308	80	0.004 ± 0.070	80		
15-16	0.010 ± 0.181	59	-0.049 ± 0.044	59		
NGC 2437						
Stetson (2000, ccd)						
11-12	0.029 ± 0.002	3	0.018 ± 0.005	3		
12-13	0.028 ± 0.014	16	0.017 ± 0.013	16		
13-14	0.029 ± 0.015	14	0.009 ± 0.018	14		
14-15	0.029 ± 0.014	15	0.002 ± 0.012	15		
15-16	0.030 ± 0.013	23	0.001 ± 0.015	23		
16-17	0.030 ± 0.021	15	0.004 ± 0.020	15		
17-18	0.019 ± 0.018	20	0.008 ± 0.031	20		
18-19	0.049 ± 0.076	14	0.001 ± 0.090	14		
19-20	0.046 ± 0.030	6	-0.053 ± 0.045	6		
Henden (2003, ccd)						
11-12	0.048 ± 0.034	10	0.001 ± 0.031	10		
12-13	0.038 ± 0.022	16	-0.005 ± 0.012	16		
13-14	0.025 ± 0.088	17	-0.031 ± 0.137	17		
14-15	0.042 ± 0.018	24	-0.014 ± 0.019	24		
15-16	0.017 ± 0.098	50	-0.011 ± 0.022	50		
16-17	-0.001 ± 0.113	92	-0.040 ± 0.084	92		
17-18	-0.004 ± 0.122	108	-0.048 ± 0.089	108		
18-19	0.029 ± 0.151	97	-0.068 ± 0.159	91		
Lynga & Palous (1987, pe)						
<10	0.041 ± 0.000	1				
10-11	0.010 ± 0.000	1				
11-12	0.014 ± 0.025	2	-0.005 ± 0.006	2		
12-13	-0.005 ± 0.000	1	-0.030 ± 0.000	1		
13-14	-0.022 ± 0.000	1	-0.045 ± 0.000	1		
Oja (1976, Pe)						
10-11	0.049 ± 0.013	4	-0.018 ± 0.010	4		
11-12	0.036 ± 0.000	1	0.001 ± 0.000	1		
12-13	0.054 ± 0.000	1	-0.021 ± 0.000	1		
Smyth & Nandy (1962, pg)						
10-11	-0.026 ± 0.067	16	-0.001 ± 0.033	15		
11-12	-0.033 ± 0.061	32	-0.009 ± 0.032	32		
12-13	-0.056 ± 0.060	61	-0.011 ± 0.032	61		
13-14	-0.090 ± 0.048	51	-0.034 ± 0.035	51		
NGC 2548						
Pesch (1961, pe)						
<9	0.047 ± 0.023	15				
9-10	0.047 ± 0.014	11				
10-11	0.051 ± 0.015	5				

Table 4—Continued

V range	$\Delta(V)$ (Mean \pm σ)	(N)	$\Delta(B - V)$ (Mean \pm σ)	(N)	$\Delta(U - B)$ (Mean \pm σ)	(N)
11-12	0.050 \pm 0.000	1				
Oja (1976, pe)						
<9	0.026 \pm 0.000	1				
9-10	0.040 \pm 0.016	2				
10-11	0.029 \pm 0.025	2				
11-12	0.066 \pm 0.058	4				
12-13	0.175 \pm 0.000	1				
13-14	0.069 \pm 0.000	1				

Table 5. Structural parameters of the target open clusters estimated from the projected radial density profile of main sequence stars having $V \leq 18$ mag.

Cluster	α_{2000} (h:m:s)	δ_{2000} (d:m:s)	Optical		2MASS	
			Core radius arcmin (pc)	Cluster extent arcmin (pc)	Core radius arcmin (pc)	Cluster extent arcmin (pc)
Be 62	01 : 01 : 15.5	63 : 56 : 17	2.2 (1.5)	10.0 (6.8)	2.5 (1.7)	12 (8.1)
NGC 1528	04 : 15 : 24.2	51 : 15 : 23	8.3 (2.6)	15.0 (4.8)	18.5 (5.9)	24 (7.6)
NGC 1960	05 : 36 : 20.8	34 : 08 : 31	3.2 (1.2)	14.0 (5.4)	3.8 (1.5)	21 (8.1)
NGC 2287	06 : 45 : 58.7	-20 : 44 : 09	1.4 (0.3)	12.0 (2.5)	12.7 (2.6)	16 (3.3)
NGC 2301	06 : 51 : 46.4	00 : 27 : 30	1.9 (0.5)	9.0 (2.3)	4.5 (1.1)	20 (5.1)
NGC 2323	07 : 02 : 47.4	-08 : 20 : 43	6.5 (1.8)	17.0 (4.7)	6.7 (1.9)	22 (6.1)
NGC 2420	07 : 38 : 24.8	21 : 34 : 30	1.4 (1.0)	10.0 (7.2)	1.3 (0.9)	9 (6.5)
NGC 2437	07 : 41 : 58.1	-14 : 49 : 28	6.8 (3.0)	20.0 (8.8)	9.6 (4.2)	25 (11.0)
NGC 2548	08 : 13 : 42.9	-05 : 46 : 37	1.5 (0.3)	8.0 (1.8)	2.4 (0.5)	8.0 (1.8)

Table 6. Recent estimates of sizes (in arcmin) of target clusters available in the literature.

Name	Kharchenko et al. (2005) r_c	Nilakshi et al. (2002) r_c	Chen et al. (2004) $r_{1/3}$	Bonatto & Bica (2005) R_{core}	r_{out}		
	r_{cl}	r_{cl}	$r_{1/3}$	R_{lim}			
NGC 1528	8.4	26.4					
NGC 1960	5.4	16.2	3.2	5.7	7.6		
NGC 2287	9.6	30.0				4.7	30.1
NGC 2301	4.8	15.0	1.9	12.0			
NGC 2323	6.0	22.2	2.6	16.7			
NGC 2420			1.5	13.2	3.7	11.6	
NGC 2437	7.2	22.8	5.2	26.6			
NGC 2548	15.0	43.8			3.9	37.8	

Table 7. The estimated parameters of the target clusters obtained in the present work using color-color diagram and color-magnitude diagrams. To determine the galactocentric distances (R_G) to the clusters, a value of 8.5 kpc has been assumed for the galactocentric distance of the Sun.

Cluster	$E(B - V)$ (mag)	Log age (yr)	Distance ($V - M_V$)	R_G (kpc)
Be 62	0.70-1.00	7.2	14.0	2.32
NGC 1528	0.26	8.6	11.0	1.09
NGC 1960	0.22	7.4	11.3	1.33
NGC 2287	0.01	8.4	9.3	0.71
NGC 2301	0.03	8.2	9.8	0.87
NGC 2323	0.20	8.0	10.5	0.95
NGC 2420	0.04	9.3	12.1	2.48
NGC 2437	0.10	8.4	11.2	1.51
NGC 2548	0.03	8.6	9.5	0.77

Table 8. Slopes of Two Color Diagrams (TCDs) for cluster Be 62, NGC 2420 and NGC 1960.

Cluster	Radius (arcmin)	$\frac{(I-V)}{(B-V)}$	$\frac{(J-V)}{(B-V)}$	$\frac{(H-V)}{(B-V)}$	$\frac{(K-V)}{(B-V)}$
Be 62	< 10	-0.99 ± 0.01	-1.78 ± 0.02	-2.29 ± 0.03	-2.49 ± 0.03
NGC 2420	< 10	-0.97 ± 0.01	-1.69 ± 0.02	-2.32 ± 0.03	-2.40 ± 0.05
NGC 1960	< 14	-1.13 ± 0.01	-1.97 ± 0.01	-2.44 ± 0.01	-2.56 ± 0.01
Normal value ¹		-1.10	-1.96	-2.42	-2.60

¹See text

Table 9. Comparison of estimates available in the literature with the present estimates.

Cluster	Observations*	E(B-V) (mag)	Distance (pc)	Age (yrs)	Reference
Be 62	pe	0.86	2050 ± 240	10^7	Forbes(1981)
	CCD	0.82	2704	10^7	Phelps & Janes(1994)
	CCD	0.70	2320	1.6×10^7	Present work
NGC 1528	pg	0.28	603	4×10^8	Francic (1989)
	CCD	0.26	1090	4×10^8	Present work
NGC 1960	CCD	0.25 ± 0.02	1318 ± 120	$16_{-5}^{+6} \times 10^6$	Sanner et al. (2000)
	CCD	0.22	1330	2.5×10^7	Present work
NGC 2287	pg	0.00	661	2×10^8	Hoag et al. (1961)
				1.7×10^8	Barbaro (1967)
	pe	0.03	758		Eggen (1974)
	pe			8×10^7	Eggen (1975)
	pe	0.01 ± 0.03	630	6.0 ± 10^7	Feinstein et al. (1978)
	pe		740	10^8	Eggen (1981)
	DDO	0.07 ± 0.02	752	$(1.1 \pm 0.4) \times 10^8$	Miriani & Ursula (1983)
	pe	0.00	675		Ianna et al. (1987)
	pe	0.064 ± 0.042	700	2×10^8	Harris et al. (1993)
	CCD	0.01	710	2.5×10^8	Present work
NGC 2301	pe	0.04	840		Nissen (1988)
	pg	0.04	794		Mohan & Sagar(1988)
		0.05	692	2×10^8	Napiwotzki et al. (1991)
	DDO	0.04	855		Twarog et al. (1997)
	CCD	0.05	832	2.5×10^8	Kim et al. (2001)
	CCD	0.03	870	1.6×10^8	Present work
NGC 2323	pg		780-860		Trumpler (1930)
	pg		500-800		Shapley (1930)
	pg		675		Collinder (1931)
	pg		520		Rieke (1935)
	pg	0.30	1210		Cuffey (1941)
	pe	0.20-0.26	1170		Hoag et al. (1961)
	pg			6×10^7	Barbaro et al. (1969)
	pg	0.33	995	1.4×10^8	Mostafa et al. (1983)
		0.04	750	$(1 - 1.4) \times 10^8$	Lynga (1984)
	pe	0.25	931	10^8	Claria et al. (1998)
	CCD	0.22	1000	1.3×10^8	Kalirai et al. (2003)
	CCD	0.20	950	10^8	Present work

Table 9—Continued

Cluster	Observations*	E(B-V)	Distance	Age	Reference
		(mag)	(pc)	(yrs)	
NGC 2420	pe&pg		2900	1.2×10^9	Sarma & Walker (1962)
	pg	0.01	2400		West (1967)
	pg			10^9	Cannon & Lloyd (1970)
	pg&pe	0.02	1905 ± 11	$3.3 \pm 0.5 \times 10^9$	McClure et al. (1974)
	pg	0.02	1900	4×10^9	McClure et al. (1978)
	CCD	0.05	2450	$3.4 \pm 0.6 \times 10^9$	Anthony-Twarog et al. (1990)
	CCD	0.05	2450	2×10^9	Lee et al. (2002)
	CCD	0.04	2480	2×10^9	Present work
NGC 2548	pe	0.04	630		Pesch (1961)
	CCD	0.03	770	4×10^8	Present work

*pe: photoelectric; pg: photographic; CCD: Charged Couple Device

Table 10. Parameters for target clusters for a mass limited sample having $M_V \leq 7$ mag.
 f_0 represents central star density of clusters.

Name	Core <i>arcmin</i> (pc)	Cluster <i>arcmin</i> (pc)	f_0 $\frac{\text{star}}{\text{arcmin}^2} (\frac{\text{star}}{\text{pc}^2})$
Be 62*	2.8 (1.9)	14.0 (9.5)	3.0 (6.6)
NGC 1528	8.3 (2.6)	15.0 (4.8)	1.7 (16.9)
NGC 1960	3.5 (1.4)	14.0 (5.4)	2.8 (18.7)
NGC 2287	1.0 (0.2)	12.0 (2.5)	2.2 (51.6)
NGC 2301	1.7 (0.4)	9.0 (2.3)	3.9 (60.9)
NGC 2323	7.2 (2.0)	17.0 (4.7)	2.5 (32.7)
NGC 2420	1.4 (1.0)	10.0 (7.2)	19.8 (38.1)
NGC 2437	8.3 (3.6)	20.0 (8.8)	3.5 (18.1)
NGC 2548	1.7 (0.4)	8.0 (1.8)	1.4 (27.9)

*for $M_V \leq 6$ mag

Table 11. Parameters of previously studied clusters (see text).

Name	Log age (yr)	Distance (kpc)	R_G (kpc)	Core radius <i>arcmin</i> (pc)	Cluster radius <i>arcmin</i> (pc)	Limiting magnitude $M_V \leq$	Reference
NGC 663	7.2	2.4	10.19	3.9 (2.7)	17.5 (12.2)	4.6	Pandey et al. (2005)
NGC 1912	8.5	1.4	9.89	4.5 (1.8)	14.0 (5.7)	6.5	Pandey et al. (in preparation)
NGC 7654	8.2	1.4	9.12	3.8 (1.6)	11.7 (4.8)	4.5	Pandey et al. (2001)
NGC 654	7.3	2.4	10.18	0.9 (0.6)	3.7 (2.6)	5.3	Pandey et al. (2005)
NGC 1907	8.5	1.8	10.33	2.0 (1.1)	6.0 (3.1)	5.0	Pandey et al. (in preparation)
King 5	9.0	1.9	10.09	0.8 (0.4)	2.8 (1.6)	5.0	Durgapal & Pandey (2001)
King 7	8.8	2.2	10.46	1.1 (0.7)	2.9 (1.9)	3.4	Durgapal & Pandey (2001)
Be 20	9.7	9.0	17.11	0.6 (1.6)	2.5 (6.6)	3.9	Durgapal & Pandey (2001)